This paper is published as part of a *Dalton Transactions* themed issue entitled:

New Talent: Americas

Guest Editors: John Arnold, Dan Mindiola, Theo Agapie, Jennifer Love and Mircea Dincă

Published in issue 26, 2012 of *Dalton Transactions*

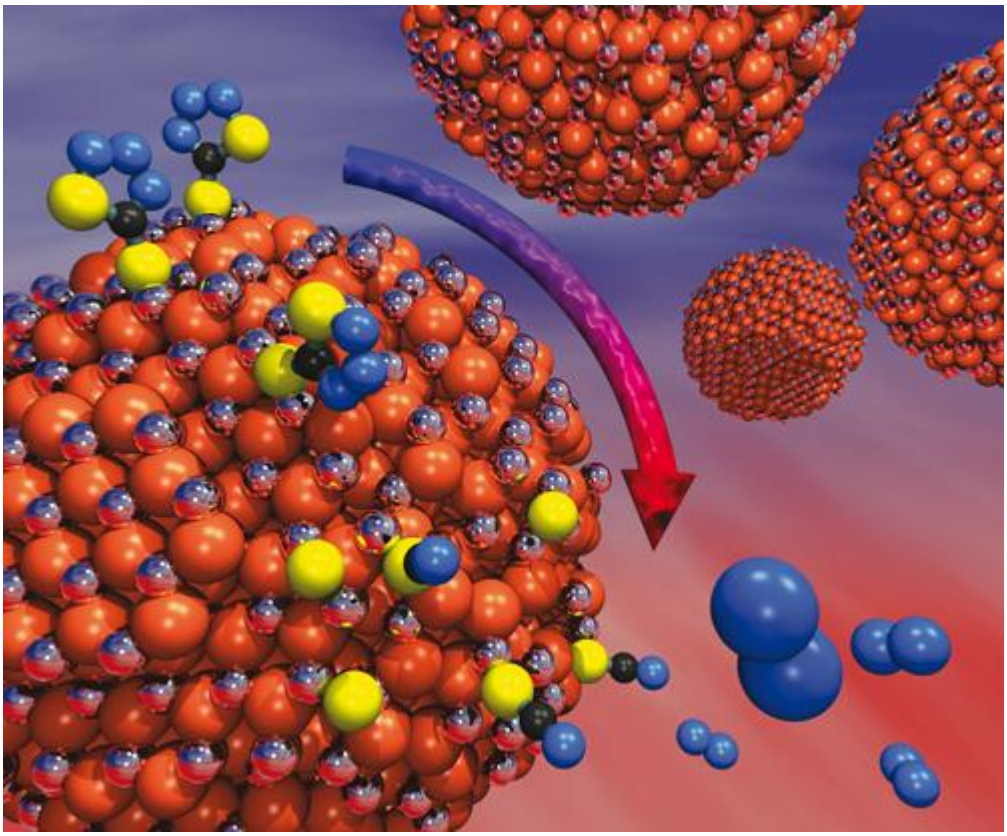

Image reproduced with permission of Richard L. Brutchey

Articles published in this issue include:

Visit the *Dalton Transactions* website for more cutting-edge inorganic chemistry
www.rsc.org/dalton

Dalton Transactions

Cite this: *Dalton Trans.*, 2012, **41**, 8162

www.rsc.org/dalton

PAPER

Quantifying factors that influence metal ion release in photocaged complexes using ZinCast derivatives†

Celina Gwizdala,[a] Charlene V. Singh,[a] Tracey R. Friss,[a] John C. MacDonald[b] and Shawn C. Burdette*[b]

Received 19th January 2012, Accepted 12th March 2012
DOI: 10.1039/c2dt30135k

Two generations of nitrobenzhydrol-based photocages for Zn^{2+} have been prepared and characterized. The first series includes the tridentate ZinCast-1 utilizes a bis-pyridin-2-ylmethyl-aniline ligand that forms a 5,5-chelate ring upon metal binding. The related photocages ZinCast-2 with a *N*-[2-(pyridine-2-yl)ethyl]-*N*-(pyridine-2-ylmethyl)aniline (5,6-chelate ring) and ZinCast-3 with a *N*,*N*-bis[2-(pyridine-2-yl)ethyl] aniline (6,6-chelate ring) were synthesized for comparative studies. The complexes formed by the ions Cu^{2+}, Zn^{2+} and Cd^{2+} with three ZinCast and their photoproducts (ZinUnc) were interrogated by UV-Vis spectroscopy. The studies indicate that ZinCast-1 forms complexes of the highest stability and ZinCast-3 exhibits the most significant changes in metal affinity upon uncaging. These results suggest that the changes in nitrogen atom donor ability as well as the initial complex stability must be considered to design a photocage with the desired properties. The composite results were used to design ZinCast-4 and ZinCast-5, the second generation photocages that incorporate an additional adjacent ether ligand into the Zn^{2+} chelator.

Introduction

Molecular photocages undergo irreversible photoreactions to trigger the release of a bioactive product.[1,2] The photocaging substituent renders the analyte inactive prior to photolysis. Upon uncaging, concentration fluxes of the released photoproduct perturb biochemical processes. The response elicited can be monitored and quantified with an orthogonal analytical technique. Uncaging can be focused in space or modulated in time the so concentration of analyte and location of its release can be controlled. A variety of bioactive molecules have been successfully incorporated into photocages facilitating the study of numerous intra- and extracellular processes.[2,3] In addition to photocaged molecules, divalent metal ion photocaged complexes have had a significant impact on the study of signal transduction.[4–6] Photocaged complexes helped provide a deeper understanding of Ca^{2+}-signaling in neurons as well as other Ca^{2+}-induced processes in non-neuronal cells. While physiological signaling roles of Ca^{2+} are well-established, similar functions for Zn^{2+} have been proposed, but not proven unequivocally.[7–9]

To facilitate the study of Zn^{2+} signaling in biology, we are developing both *Cast* and *Cleav* photocaged Zn^{2+} complexes with release mechanisms analogous to those exploited in Ca^{2+} systems.[10–12] ZinCast-1 integrates a *N*,*N*-dipicolylaniline (DPA) chelating moiety with a nitrobenzhydrol caging group.[11] Photolysis of $[Zn(ZinCast\text{-}1)(H_2O)_2]^{2+}$ is initiated by the light-induced abstraction of the benzylic hydrogen atom onto the excited nitro group yielding *aci*-nitro intermediate (Fig. 1). The intermediate decomposes to a nitrosobenzophenone photoproduct $[Zn(ZinUnc\text{-}1)]^{2+}$.[11] After photolysis, the $[Zn–DPA]^{2+}$ complex stability is decreased due to delocalization of the anilino lone pair onto the carbonyl oxygen of

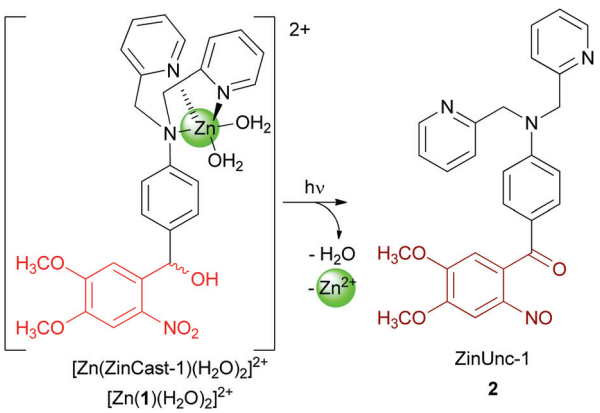

Fig. 1 Uncaging action of ZinCast-1. Upon irradiation, the nitrobenzhydrol (red) is converted into a benzophenone. The decrease in electron density on the aniline nitrogen atom due to the new resonance interaction between the aniline lone pair and the carbonyl oxygen reduces the binding affinity of the uncaged ligand.

[a]*University of Connecticut, 55 North Eagleville Road, Storrs, CT 06269-3060, USA*
[b]*Worcester Polytechnic Institute, 100 Institute Road, Worcester, MA 01609-2280, USA. E-mail: scburdette@wpi.edu*

†Electronic supplementary information (ESI) available: Additional spectroscopic data, XLfit spectral fitting protocols, complete X-ray tables and NMR spectra for new compounds. CCDC reference numbers 864178. For ESI and crystallographic data in CIF or other electronic format see DOI: 10.1039/c2dt30135k

nitrosobenzophenone. Photolysis of $[Zn(ZinCast\text{-}1)]^{2+}$ in aqueous solution (50 mM HEPES, 100 mM KCl, 20% DMSO, pH 7) leads to ~400-fold decrease in Zn^{2+} affinity.

The magnitude of the decrease in metal binding constant in ZinCast-1 after photolysis is an order of magnitude greater than that measured for nitrobenzhydrol-based Ca^{2+} photocages.[13] The efficacy of photocaged complexes for probing biological signaling is directly related to the change in metal ion affinity upon uncaging. Rationally predicting the binding affinity changes at the design stage would greatly expedite the development of photocaged complexes with the desired properties. There are well-established qualitative rules for predicting relative metal ion affinity in multidentate ligands based on chelate ring size, so study of related ZinCast derivatives could provide insight into rules for predicting photocaging properties.

Results and discussion

Design and synthesis of ZinCast photocages

The uncaging mechanism in nitrobenzhydrol-based photocages involves light-initiated formation of an *aci*-nitro intermediate that subsequently decomposes into a nitrosobenzophenone photoproduct.[15,16] In Cast[17] and Nitr[4] metal photocaged complexes, photoproduct formation triggers partial delocalization of a metal-bound aniline lone pair onto the carbonyl oxygen, which reduces the chelator's metal ion affinity. The change in metal binding equilibrium after uncaging increases the concentration of free metal ion. Practical photocages must release sufficient quantities of the metal ion analyte to trigger the biological process under investigation, so the photocage must possess a relatively high affinity before uncaging that is drastically reduced following photolysis. Initially, the binding affinity of ZinCast-1 was determined spectrophotometrically by titrating 25 μM ligand solutions with Cu^{2+}, Zn^{2+} or Cd^{2+} and monitoring the erosion of the absorption band at $\lambda \sim 260$ nm that corresponds to the metal-binding aniline group. In aqueous solution (50 mM HEPES, 100 mM KCl, pH 7.0, 20% DMSO), ZinCast-1 exhibited a K_d of 14 μM ($\log K = 4.9$) and a photolysis quantum yield of 0.7%. While the ΔK_d for the Ca^{2+} photocage Nitr-5 decreases ~40-fold upon uncaging, ZinCast-1 exhibited more dramatic changes in Zn^{2+} affinity ($\Delta K_d = 400$, $\Delta K = 2.1$). To compare photocages, the change in Zn^{2+} affinity due to photolysis of ZinCast photocage is expressed as ratio of photoproduct's stability constant (ZinUnc K_d) to the photocage's stability constant (ZinCast K_d), ΔK_d = (ZinUnc K_d)/(ZinCast K_d). All changes can also been expressed as ΔK, where ΔK = (ZinCast K)/(ZinUnc K) and $K = -\log[K_d]$.

In subsequent studies, the metal binding properties of ZinCast-1 and its photoproduct ZinUnc-1 were evaluated in EtOH and CH_3CN; in addition, the aqueous data (50 mM HEPES, 100 mM KCl, pH 7.0; "buffer") was re-acquired using EtOH as a co-solvent to avoid the spectral overlap between ZinCast-1 and DMSO (Table 1). The metal binding affinity of ZinCast-1 and ZinUnc-1 are influenced by the solvent. While Zn^{2+} affinity is the highest in CH_3CN ($K_d = 9.7$ μM), the ΔK_d is the largest in aqueous solution. Replacement of DMSO with EtOH reduces ΔK_d by a factor of ~4. The reduction in ΔK_d is caused by weakened stability constant of $[Zn(ZinCast\text{-}1)]^{2+}$ in the presence of EtOH. Changes in ligand solvation by ethanol and subsequent competition for Zn^{2+} ions by solvent molecules are hypothesized to decrease complex stability.[18] The reduced basicity of anilino nitrogen in ZinUnc-1 moderates the solvation differences and results in nearly identical binding constants in both aqueous media.

Given the solvent-based affinity variability, as well as the goal of tuning photocaged complex properties for biological applications, new ZinCast derivatives were sought to systematically study trends in metal ion binding affinity. Since ligand structure also influences metal ion affinity, studying variations of the ZinCast-1 framework provides a simple means to investigate the metal binding properties of photocaged complexes. Two complementary ZinCast derivatives where envisioned where the alkyl linker between the aniline nitrogen atom and the pyridine moiety is extended from a methylene to an ethylene spacer. This strategy provides three related photocages where the magnitude of the ΔK_d should be independent of ancillary donor groups (pyridine) and changes in the anilino nitrogen atom basicity (Fig. 2).

Zn^{2+} possesses a great degree of conformational flexibility because of its d^{10} configuration. Zn^{2+} frequently forms

Table 1 Metal binding properties of ZinCast-1[a]

		K_d			
M^{2+}	Solvent	$[M(ZinCast\text{-}1)]^{2+}$	$[M(ZinUnc\text{-}1)]^{2+}$	ΔK_d	ΔK
Zn^{2+}	CH_3CN	$(9.7 \pm 0.4) \times 10^{-6}$	$(9.7 \pm 0.2) \times 10^{-6}$	1	1.0
	EtOH	$(1.3 \pm 0.2) \times 10^{-5}$	$(3.5 \pm 0.1) \times 10^{-5}$	3	1.1
	20% EtOH–buffer	$(6.1 \pm 0.1) \times 10^{-5}$	$(5.6 \pm 0.1) \times 10^{-3}$	92	1.8
	20% DMSO–buffer	$(1.4 \pm 0.1) \times 10^{-5}$	$(5.6 \pm 0.1) \times 10^{-3}$	400	2.1
Cu^{2+}	CH_3CN	NA[b]	NA[b]	NA[b]	NA[b]
	EtOH	$(7.2 \pm 0.1) \times 10^{-6}$	$(7.2 \pm 0.3) \times 10^{-6}$	1	1
	20% EtOH–buffer	$(8.5 \pm 0.1) \times 10^{-6}$	$(1.5 \pm 0.1) \times 10^{-5}$	2	1.1
Cd^{2+}	CH_3CN	$(7.9 \pm 0.3) \times 10^{-6}$	$(3.1 \pm 0.1) \times 10^{-5}$	4	1.1
	EtOH	$(1.7 \pm 0.1) \times 10^{-5}$	$(8.2 \pm 0.2) \times 10^{-4}$	48	1.5
	20% EtOH–buffer	$(3.7 \pm 0.1) \times 10^{-4}$	$(1.8 \pm 0.1) \times 10^{-2}$	49	2.0

[a] The 1 : 1 M–L binding constants were calculated with XLfit.[14] [b] Cu^{2+} oxidizes aniline compounds in CH_3CN, so no binding constants could be measured.

complexes of both octahedral and tetrahedral geometry. Zn^{2+} complexes of the tridentate ligands bis(2-pyridylmethyl)amine (BPA) and bis(2-pyridyl-2-ethyl)amine (BPEA) have been characterized crystallographically.[19] The complexes adopt distorted mononuclear octahedral and dinuclear tetrahedral structures respectively, where the open coordination sites are occupied by water molecules and/or perchlorate anions. The distortion of the geometry in the BPA ligand structure is the result of a small bite angle (N_{py}–Zn–N_{amine} angles of 79.99 and 79.69°) that leads to formation of a long N_{amine}–Zn bond (N_{amine}–Zn 2.142 Å *vs.* N_{py}–Zn 2.080 Å). The N_{amine}–Zn bond is shorter in the BPEA complex (N_{amine}–Zn 2.022 Å *vs.* N_{py}–Zn 2.012 Å) because of the tendency of six-membered chelate rings to adopt a cyclohexane-like conformation (N_{py}–Zn–$N_{aniline}$ angles of 101.4 and 100.4°). While the Zn^{2+} complex of the hybrid *N*-[2-(pyridine-2-yl)ethyl]-*N*-(pyridine-2-ylmethyl)amine has not been characterized structurally, the N_{amine}–M bond should have an intermediate length between that of the BPA and BPEA complexes. A systematic change in N_{amine}–Zn interaction should provide a context for the Δ*K* values for different ZinCast ligands, which utilize aniline analogs of these chelators. Metal complexes with six-membered rings should experience a more profound decrease in affinity following photolysis due to greater proximity of anilino nitrogen and the metal. Conformational flexibility of Zn^{2+} as well as Cu^{2+} allows for investigation of different binding motifs in ZinCast photocages. The BPA complex with Cu^{2+} adopts distorted mononuclear square-pyramidal geometry with all three nitrogen atoms coordinating and chloride ions at the remaining two sites.[20] High proximity of the coordinating N_{py} with an average distance of N_{py}–Cu of 2.006 Å should induce high stability for Cu^{2+} complexes as well as small changes in affinity upon photolysis.

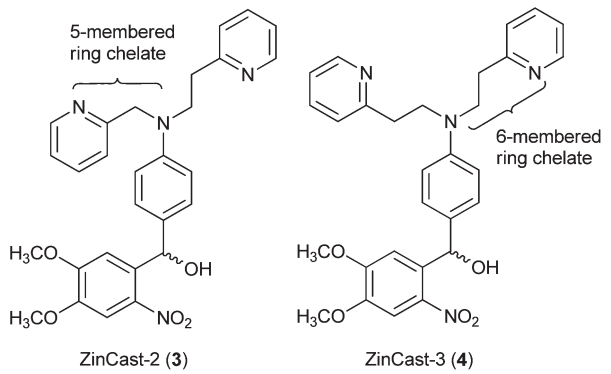

Fig. 2 Structure of ZinCast-2 and ZinCast-3. In ZinCast-1, the two methylene linkers between the nitrogen atom and the pyridine ring lead to the formation of 5,5-chelates with the guest metal ion. ZinCast-2 and ZinCast-3 systematically replace the methylene spaces with ethylene units that lead to 5,6- and 6,6-chelates upon metal ion binding.

The 5,5-ligand *N*-phenyldi(2-picolyl)aniline (**10**) and 6,6-ligand *N*,*N*-bis[2-(pyridine-2-yl)ethyl]aniline (**8**) were prepared by alkylation of aniline with picolylchloride hydrochloride and vinyl pyridine, respectively. The asymmetric 5,6-ligand was prepared by controlled addition of vinyl pyridine (**6**) to give *N*-[2-(pyridine-2-yl)ethyl]aniline (**9**) followed by reductive amination with 2-pyridinecarbaldehyde. ZinCast-1 can be prepared by the classical TMSOTf-promoted (trimethylsilyl trifluoromethanesulfonate) electrophilic aromatic substitution reaction in 58.1% yield after isolation and purification (Scheme 1).[11] The TMSOTf methodology was used to prepare ZinCast-2 and ZinCast-3 in 79.6 and 70.9% yield, respectively. The lutidine base and TMSOTf were added incrementally to maximize yields. All three compounds were isolated as yellow solids after purification by flash chromatography. ZinCast-1 also can be prepared by either a benzophenone reduction strategy or a Pd-catalyzed cross-coupling reaction described previously (Scheme 2).[11] The Pd-based methods are particularly convenient for making nitrobenzhydrol derivatives that cannot be prepared with TMSOTf methodology.

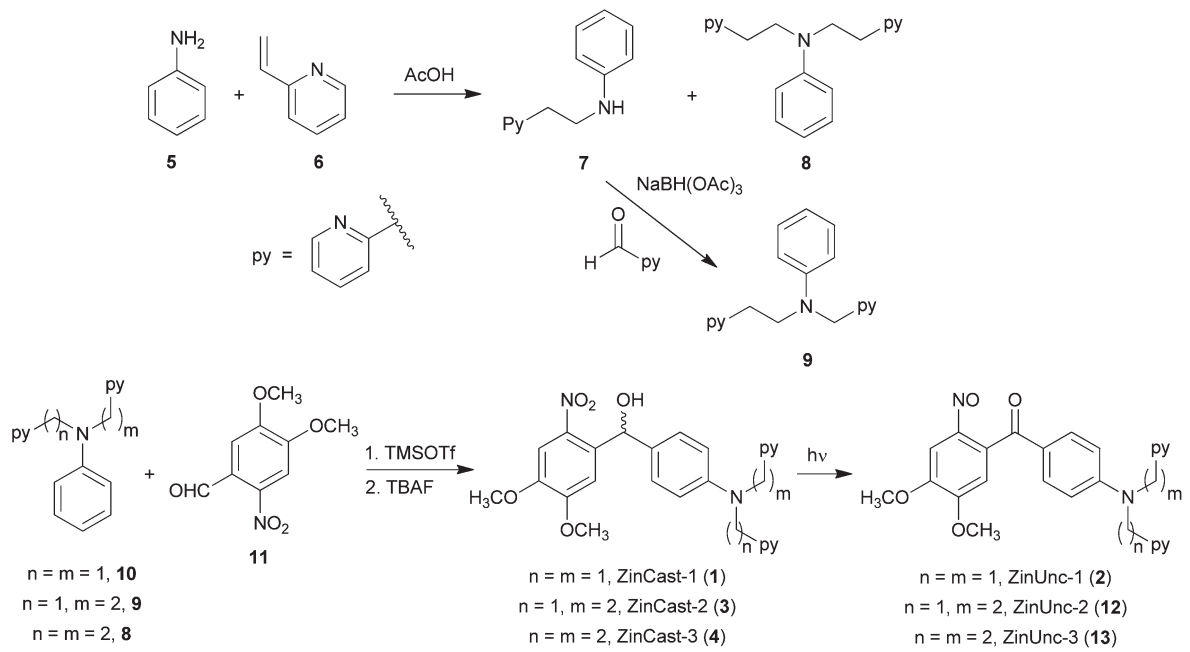

Scheme 1 Synthesis of ZinCast photocages.

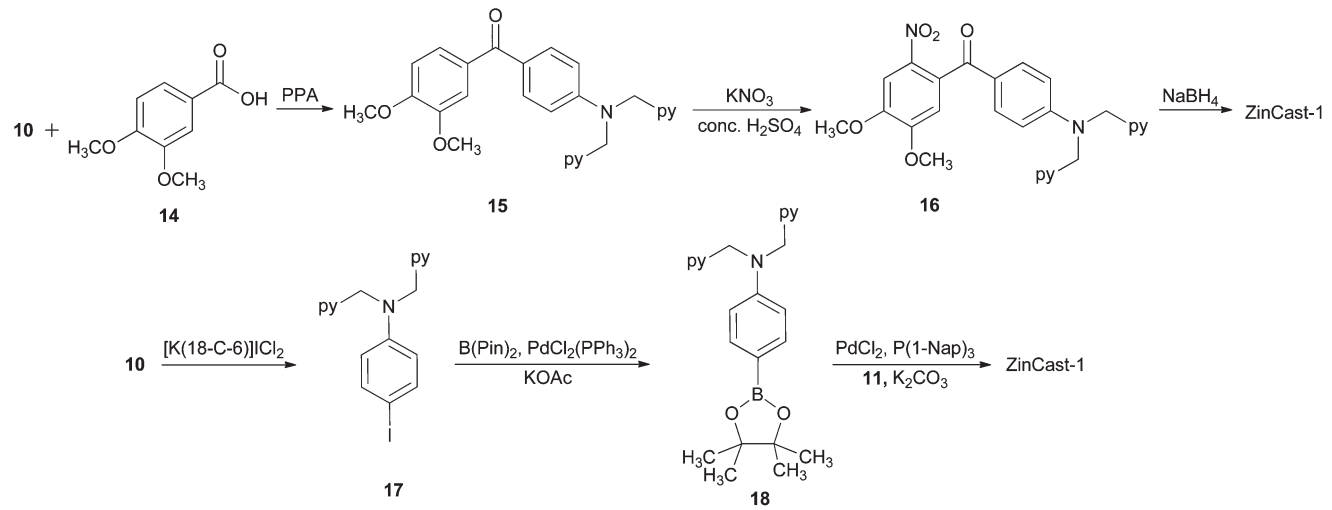

Scheme 2 Alternative synthetic pathways to ZinCast-1.

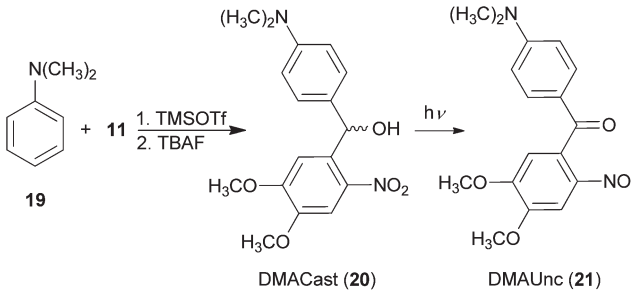

Scheme 3 Synthesis of DMACast and DMAUnc.

Table 2 pK_a of DMACast and DMAUnc[a]

Solvent	pK_a [H(DMACast)]$^+$	pK_a [H(DMAUnc)]$^+$	ΔpK_a
CH_3CN	4.8 ± 0.1	2.5 ± 0.2	1.9
EtOH	4.0 ± 0.1	~1.5	2.7
20% EtOH–buffer	4.0 ± 0.1	1.8 ± 0.2	2.2

[a] Values obtained by UV-vis spectroscopy by monitoring changes at ~265 nm for DMACast and 350 nm for DMAUnc.

Aniline basicity

The introduction of an electron withdrawing carbonyl group upon uncaging modulates the electron density on the nitrogen atom. The electron density correlates with the nitrogen atom's basicity, and insight into the variation would facilitate designing photocages with improved properties. To quantify the changes, the nitrobenzhydrol adduct of *N*,*N*-dimethylaniline (DMACast) and the corresponding photoproduct (DMAUnc) were prepared. DMACast was prepared using TMSOTf in 89.6% yield (Scheme 3), and photolysis of DMACast with 1000 W xenon lamp provided DMAUnc in 59.8% yield. DMACast allows quantification of the aniline basicity independent of the pyridine ligands, which are susceptible to protonation. In aqueous solution dimethylanilinium and pyridinium ions exhibit pK_a values of 5.1 and 5.2, respectively.[21,22] In protic solvents, the apparent pK_a of the DMACast aniline nitrogen is 4.0, which decreases to 1.8 for DMAUnc as measured by monitoring changes in the absorption spectrum at ~265 nm (Table 2). The trend in pK_a changes with DMACast is consistent with the metal ion uncaging behaviour of ZinCast-1, but the magnitude of change in ΔpK_a is larger than that for Zn^{2+} with the photocage (ΔK = 1.8) under the same conditions. Differences are even more pronounced in CH_3CN where ΔpK_a for DMACast is 1.9, but there is no measurable change in log *K* for ZinCast. The results suggest an important correlation between ligand geometric constraints, metal–nitrogen bonding interactions and ΔK.

Metal-binding properties of ZinCast photocages

Metal binding between select divalent cations and the ZinCast photocages were investigated spectrophotometrically in CH_3CN, EtOH and aqueous 20% EtOH (50 mM HEPES, 100 mM KCl, pH 7.0). Metal ion insolubility/hydrolysis combined with the weak affinity of the new photocages prevented acquisition of a complete data set in aqueous solution and ethanol (Table 3). An aniline-derived absorption band for $[Zn(ZinCast\text{-}1)]^{2+}$ was observed at λ_{max} ~ 260 nm while the same absorption band for $[Zn(ZinCast\text{-}3)]^{2+}$ was shifted to λ_{max} ~ 275 nm (Fig. 3). In addition to bathochromic shifting of the aniline-derived absorption band, a new absorption band of low extinction coefficient (ε = 6600) at λ ~ 355 nm developed. The erosion of these bands upon the addition of metal ions allowed binding affinity to be quantified. Binding studies of ZinUnc-1 and ZinUnc-2 in CH_3CN were carried out by monitoring of formation of the absorption band at ~290 nm and erosion of the benzophenone charge transfer band at ~345 nm. $[Zn(ZinUnc\text{-}3)]^{2+}$ exhibited a bathochromic shift of λ_{min} to ~360 nm and formation of two absorption bands at ~265 and ~323 nm (Fig. 4).

Metal ions binding in ZinCast-1, ZinCast-2 and ZinCast-3 photocages and the corresponding photoproducts, lead to formation of metal complexes with 5,5-, 5,6- and 6,6-chelate rings, respectively. Large and medium sized metal ions typically favor five-membered chelate rings with a small N–M–N angle (~70°) and long N–M bonds (~2.5 Å), whereas small metal ions prefer

Table 3 Metal binding properties of ZinCast-2 and ZinCast-3[a]

		K_d				K_d			
M^{2+}	Solvent	$[M(ZinCast-2)]^{2+}$	$[M(ZinUnc-2)]^{2+}$	ΔK_d	ΔK	$[M(ZinCast-3)]^{2+}$	$[M(ZinUnc-3)]^{2+}$	ΔK_d	ΔK
Zn^{2+}	CH_3CN	$(8.6 \pm 0.3) \times 10^{-6}$	$(4.8 \pm 0.1) \times 10^{-5}$	6	1.2	$(3.3 \pm 0.1) \times 10^{-5}$	$(3.8 \pm 0.1) \times 10^{-3}$	115	1.9
	EtOH	$(2.5 \pm 0.1) \times 10^{-4}$	NA[b]	NA[b]	NA[b]	$\sim 3.1 \times 10^{-3}$	NA[b]	NA[b]	NA[b]
Cu^{2+} [c]	EtOH	$(7.4 \pm 0.2) \times 10^{-6}$	$(1.1 \pm 0.1) \times 10^{-5}$	1.5	1.0	$(2.9 \pm 0.2) \times 10^{-5}$	NA[b]	NA[b]	NA[b]
Cd^{2+}	CH_3CN	$(1.3 \pm 0.1) \times 10^{-5}$	$(2.5 \pm 0.2) \times 10^{-5}$	1.9	1.1	$(1.8 \pm 0.1) \times 10^{-4}$	NA[b]	NA[b]	NA[b]
	EtOH	$(6.5 \pm 0.1) \times 10^{-4}$	NA[b]	NA[b]	NA[b]	NA[b]	NA[b]	NA[b]	NA[b]

[a] The 1 : 1 M–L binding constants were calculated with XLfit.[14] [b] M^{2+} affinity was too weak to be accurately assessed. Metal ion insolubility/hydrolysis at higher concentrations precluded accurate determination of binding affinity in aqueous conditions. [c] Cu^{2+} oxidizes aniline compounds in CH_3CN, so no binding constants could be measured.

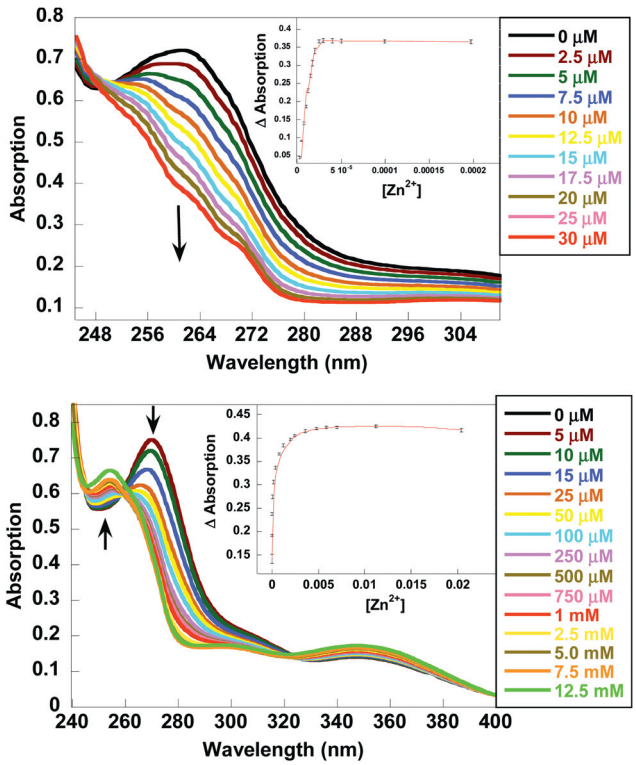

Fig. 3 Titration of 25 μM ZinCast-1 (top) and ZinCast-3 (bottom) with $Zn(ClO_4)_2$ in CH_3CN. The absorbance was fitted to a 1 : 1 binding isotherm (inset). The error bars represent the variance in the measurements over three trials.

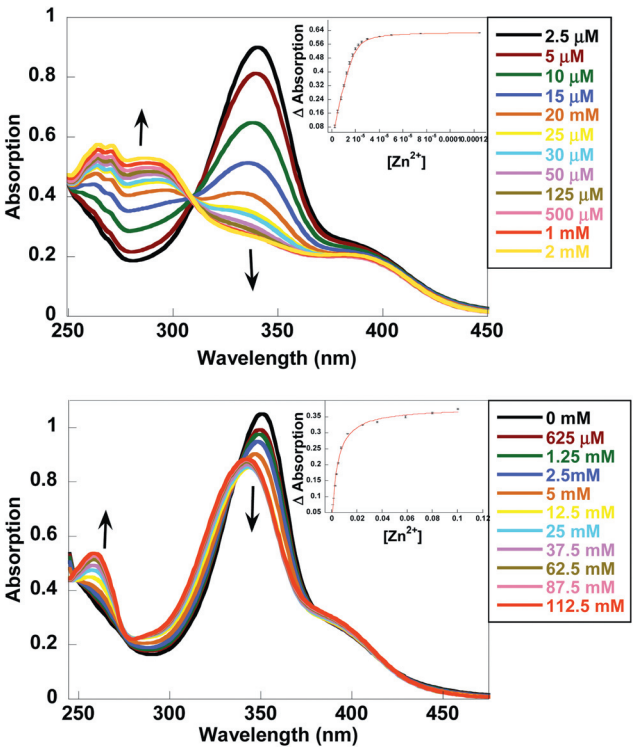

Fig. 4 Titration of 25 μM ZinUnc-1 (top) and ZinUnc-3 (bottom) with $Zn(ClO_4)_2$ in CH_3CN. The absorbance was fit to a 1 : 1 binding isotherm (inset). The error bars represent the variance in the measurements over three trials.

six-membered chelate rings with larger N–M–N angles (~100°) and a short N–M bond (~1.6 Å).[23] While these conformations reduce strain energy, they have a significant effect on the stability of the metal complexes. A medium size ion such as Zn^{2+} will prefer to coordinate a tridentate ligand with 5,5-chelate rings such as DPA. As a consequence complex stabilities increase systematically 5,5 > 5,6 > 6,6 as predicted. Increasing the length of the link between anilino nitrogen and pyridine has an overall destabilizing effect on metal complexes of ZinCast photocages. This effect is even more pronounced for the metal complexes of ZinUnc which results in steadily increasing change in metal affinity (ΔK_d) upon uncaging.

Comparison of bond distances in Zn^{2+} complexes with BPA and BPEA shows a more pronounced elongation of the $N_{aniline}$–Zn bond (Δ = 0.120 Å) than in N_{py}–Zn (Δ = 0.066 Å),[19] which is consistent with similar $[Zn(DPA)]^{2+}$ structures.[24–26] These results suggest that the $N_{aniline}$–Zn bond in $[Zn(ZinCast-1)]^{2+}$ might be longer than the $N_{aniline}$–Zn bond in $[Zn(ZinCast-3)]^{2+}$ complex. Since stability of the studied photocaged complexes decreases in opposing direction to the shortening of the $N_{aniline}$–Zn bond, we hypothesize the N_{py}–Zn interactions are more significant to complex stability in ZinCast-1. This behavior is also consistent with the trends in ΔK_d. A longer $N_{aniline}$–Zn bond in ZinUnc-1 would significantly reduce the effect of decreased electron availability after uncaging which leads to a small ΔK_d

Table 4 Metal binding properties of ZinCast-4 and ZinCast-5[a]

		K_d				K_d			
M^{2+}	Solvent	$[M(ZinCast\text{-}4)]^{2+}$	$[M(ZinUnc\text{-}4)]^{2+}$	ΔK_d	ΔK	$[M(ZinCast\text{-}5)]^{2+}$	$[M(ZinUnc\text{-}5)]^{2+}$	ΔK_d	ΔK
Zn^{2+}	EtOH	$(1.2 \pm 0.2) \times 10^{-5}$	$(1.1 \pm 0.1) \times 10^{-5}$	1	1.0	$(1.5 \pm 0.2) \times 10^{-5}$	NA[b]	NA[b]	NA[b]
	EtOH–buffer	$(1.1 \pm 0.3) \times 10^{-5}$	$(5.6 \pm 0.1) \times 10^{-5}$	4	1.2	$(1.4 \pm 0.3) \times 10^{-5}$	NA[b]	NA[b]	NA[b]
Cu^{2+}	EtOH	$(7.5 \pm 0.1) \times 10^{-6}$	$(8.2 \pm 0.1) \times 10^{-6}$	1	1.0	$(1.4 \pm 0.1) \times 10^{-5}$	NA[b]	NA[b]	NA[b]
Cd^{2+}	EtOH	$(7.0 \pm 0.2) \times 10^{-6}$	$(1.1 \pm 0.1) \times 10^{-5}$	2	1.0	$(9.8 \pm 0.2) \times 10^{-6}$	NA[b]	NA[b]	NA[b]
	EtOH–buffer	$(9.8 \pm 0.1) \times 10^{-6}$	$(4.9 \pm 0.1) \times 10^{-5}$	4	1.2	$(1.3 \pm 0.1) \times 10^{-5}$	NA[b]	NA[b]	NA[b]

[a] The 1 : 1 M–L binding constants were calculated with XLfit.[14] [b] The ZinCast-5 photoproduct could not be isolated for analysis of its metal binding properties.

and relatively high affinity for Cu^{2+} and Zn^{2+}. In contrast, for $[Zn(ZinUnc\text{-}3)]^{2+}$ where the $N_{aniline}$–M is predicted to be shorter, the availability of the lone pair of electrons is enhanced. Subsequent photolysis and delocalization of the lone pair on the carbonyl oxygen leads to more efficient release of the coordinated metal and large ΔK_d. Ligands with 5,5-chelates effectively coordinate metal ion with all three nitrogen atoms. Inclusion of an additional carbon in the backbone of the ligand enhances the contribution of the $N_{aniline}$–Zn bond to complex stability.

Stability constants for complexes of ZinCast and ZinUnc follow the hard soft acid base (HSAB) principle and conform to the Irving–Williams series. All stability constants decrease according to the following pattern: $Cu^{2+} > Zn^{2+} > Cd^{2+}$, however change in affinity ΔK_d has an opposing trend: $Cu^{2+} < Zn^{2+} < Cd^{2+}$. This pattern implies that as the affinity for the metal increases, coordination by the pyridyl nitrogen atoms becomes more significant. While the pK_a of the anilino nitrogen is affected by photolysis of the all the ZinCast photocages, the reduced nucleophilicity will only diminish cation affinity if the aniline nitrogen atom and the metal ion guest are in close proximity (Table 4).

Design of second-generation ZinCast photocages

While changing ZinCast-1 structure led to improvements in ΔK_d, increasing the Zn^{2+} affinity while preserving a relatively high ΔK_d is necessary to apply ZinCast photocages to problems in biology. Cells typically maintain $[Zn^{2+}]$ concentration as sub-nM levels, and an effective photocage cannot perturb this homeostasis prior to uncaging. We reasoned that increasing the denticity of ZinCast-1 by incorporating a weakly coordinating methyl ether would lead to increased complex stability without compromising metal ion release upon uncaging. The high affinity observed in structurally related fluorescent sensors for Zn^{2+} with multiple additional chelating ligands suggest that additional ligands appended to the ether oxygen might impair metal ion release.[27,28] The second-generation photocage ZinCast-4 that incorporates an aryl ether ligand with the DPA ligand was prepared by Pd-catalyzed cross-coupling between the boronic ester of the ligand and the corresponding aldehyde in 43% yield (Scheme 4).

In all the Cast and Cast-like photocaged complexes described to date, the aniline nitrogen occupies the position *para* to the pendent caging group. Although metal ion release relies primarily on resonance interactions between the aniline lone pair and the carbonyl oxygen formed upon photolysis, an analogous resonance interaction between the aniline lone pair and the *aci*-nitro intermediate generated upon exposure to light appears to reduce the quantum yield of uncaging.[29] The competing considerations of high metal ion affinity and maximizing the uncaging efficiency make the design of photocages that use this release mechanism particularly challenging. Since inductive effects might also contribute to changes in metal ion affinity, ZinCast-5, where the positions of the DPA and methoxy group were exchanged, also was prepared for analysis (Scheme 4). With the less electron-donating methoxy group in the *para* position, we hypothesized that the quantum yield might be improved without significantly compromising the ΔK_d.

The binding affinities of ZinCast-4 and ZinCast-5 solutions were measured for the same metal ions and under the same conditions as the original ZinCast photocages. Since ZinCast-1 exhibited no measurable ΔK_d in CH_3CN, no analogous measurements were performed for ZinCast-4 and ZinCast-5. While the photoproduct of ZinCast-4 photocage, ZinUnc-4, could be synthesized on a preparative scale to allow for direct determination of metal ion affinities, decomposition of ZinUnc-5 made isolation of the photoproduct impossible. Unlike the first-generation ZinCast photocages, which exhibit much lower metal ion affinities in aqueous solution, the stability of ZinCast-4 and ZinCast-5 complexes are insensitive to increasing solvent polarity. This suggests that ZinCast-4 and ZinCast-5 are less solvated than the original photocages, which leads to decreased competition for binding.

While $[Zn(ZinCast\text{-}4)]^{2+}$ possess a six-fold increase in Zn^{2+} affinity in aqueous solution compared to $[Zn(ZinCast\text{-}1)]^{2+}$ only small changes in affinity occur following photolysis. X-Ray crystallography of an analogous model ligand suggests that any Zn–O_{ether} interaction in solution, if any, is probably weak since no coordination is observed in the solid state (Fig. 5). Analogous Cu^{2+} complexes also exhibit no ether coordination.[30] Instead of coordination, the methoxy group may increase the electron density of the aryl ring and therefore modulate the anilino nitrogen–carbonyl resonance interaction. While ΔK_d for ZinCast-5 could not be determined, without a resonance interaction with the aniline lone pair, it is unlikely the ΔK_d would be large.

In contrast to the Zn^{2+} complexes, Cd^{2+} appears to benefit from coordination to the methoxy oxygen. The $[Cd(ZinCast\text{-}4)]^{2+}$ and $[Cd(ZinCast\text{-}5)]^{2+}$ complexes possess stability constants that are

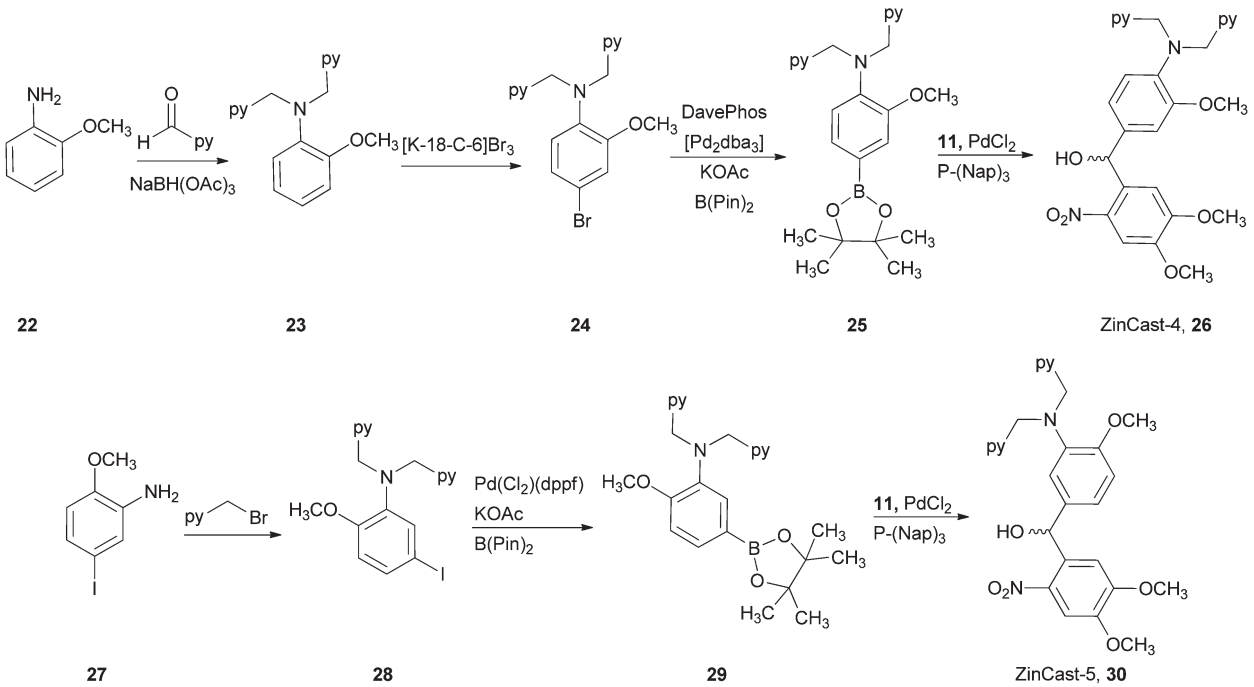

Scheme 4 Synthesis of ZinCast-4 and ZinCast-5.

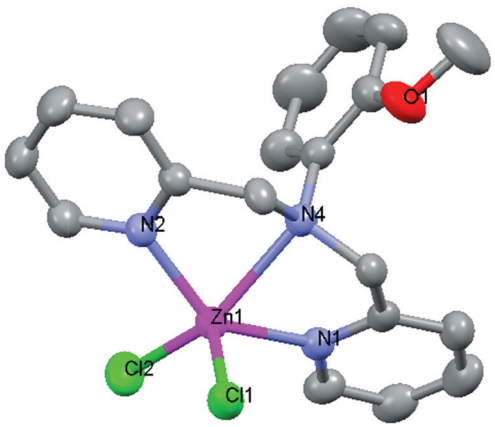

Fig. 5 ORTEP diagram of ZinCast-4 model complex [Zn(**23**)]Cl_2 showing 50% thermal ellipsoids and selected atom labels. Hydrogen atoms are omitted for clarity.

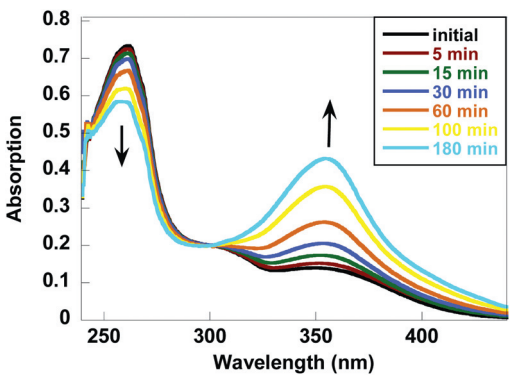

Fig. 6 Photolysis of ZinCast-1 in CH_3CN. Irradiation at 350 nm leads to the erosion of the absorption band a 270 nm associated with ZinCast-1 and the concurrent formation of a band at 350 nm characteristic of the benzophenone photoproduct ZinUnc-1.

~40 fold higher than the K_d for [Cd(ZinCast-1)]$^{2+}$ in aqueous solution. The major disadvantage of the increased stability for these complexes is lack of significant reduction in Cd^{2+} affinity in the corresponding photoproducts. The pattern of enhanced stability of metal-cage complex and consequential decrease in ΔK_d seen for the discussed Cd^{2+} complexes supports the hypothesis that the addition of strongly coordinating pending groups to ZinCast photocages would significantly compromise Zn^{2+} ion release efficiency.

Uncaging of ZinCast photocages

The efficiency of the light-induced conversion of nitrobenzhydrol based photocages of ZinCast-1, -2, -3 into the corresponding nitrosobenzophenones can be evaluated spectrophotometrically. The uncaging process can be quantified by monitoring changes in absorption of ZinCast and the corresponding photoproduct ZinUnc (Fig. 6). Quantum yields (Φ) were determined by irradiating 25 μM solutions of free ZinCast photocages in three solvent systems with a 150 W source (λ = 350 nm). Measurement of changes at λ_{max} ~ 350 nm due to formation of ZinUnc as well as calibration of the light intensity by iron oxalate actinometry allowed for calculation of Φ for the conversions. All three ZinUnc derivatives were prepared in bulk by photolysis of the ZinCast photocages in CH_3CN followed by column chromatography (Scheme 1). Working with ZinUnc on a preparative scale allows for accurate determination of extinction coefficients as well as metal binding constants.

The Φ obtained for all three apo ZinCast derivatives were <1% in CH_3CN and buffered aqueous solution, but slightly higher in EtOH (Table 5). In the presence of Zn^{2+}, the Φ of

Table 5 Quantum yields of ZinCast and DMACast compounds. Solvents not shown when values could not be determined because of Zn^{2+} ion insolubility/hydrolysis

Compound	Solvent	$\Phi_{photolysis}$ (%)	$\varepsilon_{\lambda=350\ nm}$/ $cm^{-1}\ M^{-1}$	Efficiency, $\Phi\varepsilon$
ZinCast-1	CH_3CN	0.7 ± 0.3	5300	37
	EtOH	1.6 ± 0.7	5000	80
	EtOH–buffer	0.7 ± 0.1	5600	39
ZinCast-2	CH_3CN	0.5 ± 0.1	5400	27
	EtOH	1.5 ± 0.2	5200	78
	EtOH–buffer	0.4 ± 0.1	5100	20
ZinCast-3	CH_3CN	0.6 ± 0.1	5600	34
	EtOH	1.5 ± 0.1	5200	78
	EtOH–buffer	0.2 ± 0.1	5700	11
DMACast	CH_3CN	0.6 ± 0.1	5500	33
	EtOH	1.5 ± 0.1	5200	78
	EtOH–buffer	0.6 ± 0.1	6000	36
$[Zn(ZinCast\text{-}1)]^{2+}$	CH_3CN	0.3 ± 0.1	5400	16
	EtOH	2.2 ± 0.2	5100	112
	EtOH–buffer	0.5 ± 0.3	5700	28
$[Zn(ZinCast\text{-}2)]^{2+}$	CH_3CN	0.4 ± 0.2	5600	22
	EtOH	1.8 ± 0.2	5300	95
$[Zn(ZinCast\text{-}3)]^{2+}$	CH_3CN	1.2 ± 0.2	6300	76
$[H(DMACast)]^{+}$	CH_3CN	5.1 ± 0.6	6600	337
	EtOH	1.9 ± 0.1	5300	101

ZinCast-3 doubled in CH_3CN. The low efficiency of photolysis in nitrobenzhydroyl photocaged complexes has been attributed to a resonance interaction between the anilino nitrogen and *aci*-nitro intermediate, which perturbs the uncaging process.[12,29] The predicted short $N_{aniline}$–Zn bond in $[Zn(ZinCast\text{-}3)(H_2O)_2]^{2+}$ would make the aniline lone pair less likely to engage in resonance interactions. A decrease in resonance interaction is consistent with the higher Φ measured for the complex. The same reasoning provides insight into the Φ obtained for DMACast and $[H(DMACast)]^{+}$, where the addition of HCl increases photolysis efficiency 7-fold. Like metal ion binding, protonation of the anilino nitrogen would engage the aniline lone pair in a bonding interaction inhibiting its engagement in resonance interactions.

While formation of photoproducts was followed with UV-Vis spectroscopy for the first-generation compounds initially, quantitative analysis of photolysis Φ was repeated by HPLC. The average Φ for ZinCast-1, -2 and -3 is the same as the Φ obtained for ZinCast-4 (0.6 ± 0.2), suggesting that addition of methoxy group to ZinCast-1 has minimal influence on photolysis efficiency. Changing the position of the methoxy group from *meta* to *para* appears to reduce resonance with the *aci*-nitro intermediate and increases the quantum yield. ZinCast-5 possesses the highest quantum yield of all the photocages screened (Φ = 1.0 ± 0.1).

To further understand the contribution of the resonance interaction between the *aci*-nitro intermediate and differently substituted aryl groups to quantum yields, *m*-OMeCast and *m*-DMACast were prepared by Pd cross-coupling reaction from the corresponding boronic acids (Scheme 5). Changes in Φ for all four photocages vary slightly depending on relative position

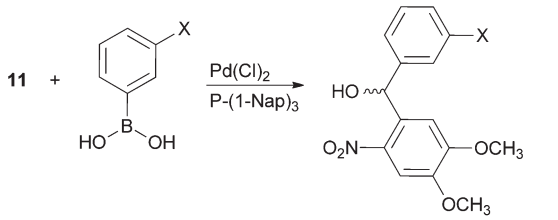

X = OCH_3, **31** X = OCH_3, *m*-OMeCast (**33**)

X = $N(CH_3)_2$, **32** X = $N(CH_3)_2$, *m*-DMACast (**34**)

Scheme 5 Synthesis of *m*-OMeCast and *m*-DMACast.

of the methoxy group. *m*-DMACast with an electron donating nitrogen in *meta* position experiences the lowest Φ (0.3 ± 0.1); however, like ZinCast-5, *m*-DMACast undergoes a secondary reaction process following photolysis that makes direct comparisons of Φ difficult. Substitution of dimethylamine for a methoxy group leads to increase in Φ (0.8 ± 0.2), which correlates with previously observed trend in Φ change as a function of the substituent's electron donating ability. UV-Vis spectra of first and second generation photocages share the same spectral features with absorption features at ~255, 300 and 345 nm. A stronger absorption of light at 255 nm may account for the larger Φ measured for ZinCast-5 and *m*-OMeCast, while increased absorption at $\lambda \sim 300$ nm seems to be associated with the unstable photoproducts of ZinCast-5 and *m*-DMACast that undergo rapid secondary reactions. The two photocages with aniline groups in the *meta* position initially appear to form nitrosobenzophenone based photoproducts initially, but instability of these compounds leads to the formation of unidentified fluorescent compounds.

Conclusion

We have synthesized three ZinCast photocages based on tridentate ligands of bis(pyridin-2-ylmethyl)aniline ligand (5,5 chelate ring), *N*-[2-(pyridine-2-yl)ethyl]-*N*-(pyridine-2-ylmethyl)aniline (5,6 chelate ring) and *N*,*N*-bis[2-(pyridine-2-yl)ethyl]aniline to study how size of the chelate rings effect metal ion binding affinity. While the 5,5 chelate rings impart complex stability, the tighter binding also compromises Zn^{2+} release upon uncaging. ZinCast-3, which utilizes the 6,6-metal chelate, exhibits the biggest changes in affinity upon photolysis. We hypothesize that a shorter N_{amine}–M bond in ZinCast-3 induces greater dependability of the complex on the lone pair of electrons of the anilino nitrogen. Delocalization of this pair of electrons onto carbonyl oxygen in the photoproduct significantly reduces stability of the metal complex and leads to larger ΔK_d.

Addition of methoxy ligands to the ZinCast-1 affords ZinCast-4 and ZinCast-5; however, no significant perturbation in the metal binding affinity or the efficiency of photolysis was observed. The latter conclusion is supported by investigation into the photochemistry of the model complexes *m*-OMeCast and *m*-DMACast and DMACast that all uncage with similar quantum yields. While the low quantum yield and weak affinity compromise the ability of these ZinCast ligands to buffer Zn^{2+} under physiologically relevant conditions, these studies provide an important roadmap for designing photocaged complexes with

predictable properties. The application of these findings to the construction of photocages for biological applications is ongoing.

Experimental

Synthesis

General experimental. All materials were in the highest purity commercially available from Acros Organic or TCI America. Solvents were sparged with argon and dried in Seca Solvent Purification System. *N*-Phenyldi(2-picolyl)aniline (**10**),[11] *N*-[2-(pyridine-2-yl)ethyl]aniline (**7**),[31] *N*,*N*-bis[2-(pyridine-2-yl)ethyl]aniline (**8**),[32] and [4-(dimethylamino)phenyl](4,5-dimethoxy-2-nitrophenyl)methanol (**20**, DMACast)[29] were prepared according to known procedures. All chromatography and TLC were performed on silica from Silicycle or activated basic alumina from Acros Organics. ^{1}H and ^{13}C NMR spectra were recorded with Bruker 400 MHz spectrometer and referenced to $CDCl_3$. IR spectra were recorded on a Nicolet 205 FT-IR instrument and samples were analyzed as KBr pellets. High-resolution mass spectra were obtained on micromass Q-Tof-2^{TM} mass spectrometer operating in positive ion mode. The instrument was calibrated with Glu-fibrinopeptide B 10 pmol μL^{-1} by using a 50 : 50 solution of CH_3CN–H_2O with 0.1% acetic acid.

*[4-(Bis-pyridin-2-ylmethylamino)phenyl](4,5-dimethoxy-2-nitrophenyl) methanol (**1**, ZinCast-1).* Trimethylsilyl trifluoromethanesulfonate (TMSOTf) (1.25 mL, 6.88 mmol) was added dropwise to a mixture of **4** (0.373 g, 1.36 mmol), 6-nitroveratraldehyde (**11**, 0.372 g, 1.76 mmol) and 2,6-lutidine (0.94 mL, 8.13 mmol) in degassed CH_2Cl_2. The resulting solution was stirred for 12 h. Tetrabutylammonium fluoride (TBAF) in THF (1 M, 4.30 mL, 15.4 mmol) was added to the reaction mixture. After 30 min the solvent was removed under reduced pressure and product was purified on basic alumina with EtOAc affording a yellow solid (0.383 g, 58.1%). Mp 113–114 °C. ^{1}H NMR ($CDCl_3$, 400 MHz) δ 8.55 (2 H, d, J = 4.0 Hz), 7.60 (3 H, m), 7.41 (1 H, s), 7.21 (2 H, d, J = 8.0 Hz), 7.15 (2 H, t, J = 8.0 Hz), 7.09 (2 H, d, J = 12.0 Hz), 6.61 (2 H, d, J = 8.0 Hz), 6.47 (1 H, s), 4.76 (4 H, s), 3.95 (3 H, s), 3.92 (3 H, s), 2.93 (1 H, s). ^{13}C NMR ($CDCl_3$, 100 MHz) δ 158.6, 153.4, 149.7, 147.9, 147.7, 139.9, 136.9, 134.8, 130.8, 128.4, 122.1, 120.8, 112.4, 110.1, 108.1, 77.3, 71.3, 57.3, 56.4, 56.3 ppm. IR (KBr) 3285, 2939, 2848, 1610–1570, 1517, 1473–1463, 1439, 1380, 1353, 1326, 1266, 1219, 1181, 1154, 1061 cm^{-1}. HRMS (+ESI): Calc. for MH^+, 487.1981. Found, 487.1946.

*(4,5-Dimethoxy-2-nitrophenyl)(4-{[2-(pyridine-2-yl)ethyl](pyridine-2-ylmethyl)amino}phenyl)methanol (**3**, ZinCast-2).* Synthesis of ZinCast-2 followed the same procedure as ZinCast-1 using **9** (0.58 g, 2.0 mmol), **11** (0.55 g, 2.6 mmol), lutidine (0.35 mL, 3.0 mmol), TMSOTf (0.47 mL, 2.59 mmol), 1 M TBAF in THF (6.00 mL, 6.00 mmol). The product was purified on basic alumina with neat EtOAc affording a yellow solid (0.801 g, 79.6%). Mp 60–62 °C. ^{1}H NMR ($CDCl_3$, 400 MHz) δ 8.49 (2 H, d, J = 4 Hz), 7.52 (4 H, m), 7.08 (6 H, m), 6.62 (2 H, d, J = 8 Hz), 6.46 (1 H, s), 4.49 (2 H, s), 3.95 (3 H, s), 3.91 (3 H, s), 3.84 (2H, t, J = 8 Hz), 3.08 (3 H, m). ^{13}C NMR ($CDCl_3$, 100 MHz) δ 159.5, 159.3, 153.6, 149.7, 147.9, 147.7, 140.2, 136.9, 136.7, 135.2, 130.4, 128.6, 123.8, 122.1, 121.7, 120.9 112.3, 110.4, 108.4, 71.5, 57.1, 56.6, 52.1, 36.0 ppm. IR (KBr) 3100, 3008, 2934, 1612, 1591, 1571, 1516, 1470, 1435, 1392, 1329, 1270, 1206, 1179, 1150, 1063, 987, 815, 796, 748 cm^{-1}. HRMS (+ESI): Calc. for MH^+, 501.2138. Found, 501.2107.

*(4-{Bis[2-(pyridine-2-yl)ethyl]amino}phenyl)(4,5-dimethoxy-2-nitrophenyl)methanol (**4**, ZinCast-3).* Synthesis of ZinCast-3 followed the same procedure as ZinCast-1 using **8** (0.188 g, 0.620 mmol), **11** (0.170 g, 0.805 mmol), 2,6-lutidine (0.11 mL, 0.95 mmol), TMSOTf (0.15 mL, 0.83 mmol), 1 M TBAF in THF (1.86 mL, 1.86 mmol). The product was purified on basic alumina (1 : 4 hexanes–EtOAc) affording orange solid (0.226 g, 70.9%). Mp 55–57 °C. ^{1}H NMR ($CDCl_3$, 400 MHz) δ 8.50 (2 H, d, J = 4 Hz), 7.59 (1 H, s), 7.51 (2 H, t, J = 8 Hz), 7.46 (1 H, s), 7.16 (2 H, d), 7.07 (4 H, m), 6.71 (2 H, d, J = 8 Hz), 6.49 (1 H, s), 3.97 (3 H, s), 3.92 (3 H, s), 3.61 (4 H, t, J = 12 Hz), 3.03 (1 H, s), 2.95 (4 H, t, J = 12 Hz). ^{13}C NMR ($CDCl_3$, 100 MHz) δ 159.9, 153.7, 149.8, 148.0, 147.4, 140.3, 136.7, 135.5, 129.9, 128.8, 123.8, 121.7, 112.2, 110.5, 108.5, 71.6, 56.8, 56.7, 51.5, 36.2 ppm. IR (KBr) 3105, 2933, 1611, 1517, 1436, 1358, 1329, 1270, 1207, 1177, 1063 cm^{-1}. HRMS (+ESI): Calc. for MH^+, 515.2294. Found, 515.2288.

N-*[2-(Pyridine-2-yl)ethyl]*-N-*(pyridine-2-ylmethyl)aniline (**9**).* 2-Pyridinecarbaldehyde (0.55 mL, 4.88 mmol) was added to a stirring solution of **7** (0.645 g, 3.25 mmol) in 30 mL of dichloroethane. After 30 min, $NaBH(OAc)_3$ (1.03 g, 4.88 mmol) and an additional 30 mL of dichloroethane was added. The reaction mixture was stirred for 12 h at room temperature, the solvent was removed under reduced pressure, 60 mL of water was added and the pH of the aqueous mixture was adjusted to between 8–9 with 5 M NaOH. The product was extracted into CH_2Cl_2 (3 × 60 mL) and the combined organic fractions were dried over anhydrous Na_2SO_4, filtered and the solvent was removed. Flash chromatography on silica with a solvent gradient (EtOAc to 50 : 1 EtOAc–CH_3OH) yielded the product as a clear yellow oil (0.801 g, 85.2%). ^{1}H NMR ($CDCl_3$, 400 MHz) δ 8.54 (2 H, d, J = 4 Hz), 7.52 (2 H, m, J = 8 Hz), 7.18 (2 H, t, J = 8 Hz), 7.11 (4 H, m), 6.70 (3 H, m), 4.56 (2 H, s), 3.90 (2 H, t, J = 8 Hz), 3.15 (2 H, t, J = 8 Hz). ^{13}C NMR ($CDCl_3$, 100 MHz) δ 159.7, 159.6, 149.8, 149.7, 147.9, 136.9, 136.6, 129.5, 123.8, 122.0, 121.6, 120.8, 116.8, 112.4, 57.2, 52.0, 36.1 ppm. IR (KBr) 3061, 3008, 2926, 1590, 1570, 1506, 1472, 1433, 1390, 1353, 1273, 1244, 1198, 1162, 1147, 1049, 989, 943, 747, 694 cm^{-1}. HRMS (+ESI): Calc. for MH^+, 312.1477. Found, 312.1463.

*[4-(Bis-pyridin-2-ylmethylamino)phenyl](3,4-dimethoxyphenyl) methanone (**15**).* A 10 g potion of 84% polyphosphoric acid (PPA) was added to a suspension of 2,3-dimethoxybenzoic acid (**14**, 1.09 g, 5.99 mmol) in 5 mL of CH_2Cl_2, and the resulting mixture was heated to 80 °C. Compound **3** (1.65 g, 5.99 mmol) was added to the red reaction mixture, which was stirred for an additional 2 h at 80 °C. The dark red reaction mixture was cooled to 0 °C and the PPA was neutralized by adding 6 M NaOH dropwise until the solution reached a pH of 9–10. The product was extracted into CH_2Cl_2 (3 × 50 mL) and the combined organic extracts were dried over Mg_2SO_4. Flash chromatography on basic alumina with diethyl ether afforded **4** as a white solid (2.24 g, 84.9%). Mp 135–136 °C. ^{1}H NMR ($CDCl_3$, 400 MHz) δ 8.60 (2 H, d, J = 4.0), 7.70 (2 H, d, J = 8.0 Hz), 7.64 (2 H, t, J = 8.0 Hz), 7.37 (1 H, s), 7.32 (1 H, d, J = 8.0

Hz), 7.24 (2 H, d, J = 8.0 Hz), 7.20 (2 H, t, J = 8.0 Hz), 6.85 (1 H, d, J = 8.0 Hz), 6.75 (2 H, d, J = 8.0 Hz, ArH), 4.90 (4 H, s, N–CH_2–Py), 3.92 (3 H, s, OCH_3), 3.90 (3 H, s, OCH_3). ^{13}C NMR ($CDCl_3$, 100 MHz) δ 194.1, 157.9, 152.3, 151.8, 150.1, 149.0, 137.1, 132.7, 131.6, 127.0, 124.5, 122.5, 120.9, 112.5, 111.7, 109.9, 57.4, 56.2 ppm. IR (KBr) 3076, 3007, 2963, 2834, 1625, 1461, 1437, 1414, 1390, 1365, 1340, 1321, 1038, 992, 958, 941, 877, 841, 818, 702, 627, 510, 406 cm^{-1}. HRMS (+ESI): Calc. for MH^+, 440.1974. Found, 440.2010.

*[4-(Bis-pyridin-2-ylmethylamino)phenyl](4,5-dimethoxy-2-nitrophenyl)methanone (**16**).* $Cu(NO_3)_2{\cdot}2.5H_2O$ (1.27 g, 5.46 mmol) was added to a solution of **15** (1.60 g, 3.64 mmol) in acetic anhydride (10 mL) at 0 °C and the reaction mixture was stirred for 12 h. Ice and 25 mL of 0.4 M EDTA were added to the solution and the pH was adjusted to 9 with 6 M NaOH. The product was extracted into CH_2Cl_2 (3 × 50 mL) and the combined organic extracts were dried over Mg_2SO_4. Flash chromatography on alumina (17 : 3 CH_2Cl_2–EtOAc) followed by recrystallization from toluene yielded **16** as a white solid (1.00 g, 56.7%). Mp 200–201 °C. ^{1}H NMR ($CDCl_3$, 400 MHz) δ 8.59 (2 H, d, J = 4.0 Hz), 7.69 (1 H, s), 7.64 (2 H, t, J = 8.0 Hz), 7.58 (2 H, d, J = 12.0 Hz), 7.19 (4 H, m), 6.78 (1 H, s), 6.69 (2 H, d, J = 12.0 Hz), 4.87 (4 H, s), 3.99 (3 H, s), 3.92 (3 H, s). ^{13}C NMR ($CDCl_3$, 100 MHz) δ 191.7, 157.5, 154.0, 152.8, 150.2, 149.4, 137.2, 131.9, 131.6, 125.5, 122.6, 120.9, 112.0, 110.2, 107.1, 57.3, 56.8, 56.7 ppm. IR (KBr) 3076, 3007, 2963, 2834, 1647, 1592–1570, 1548, 1522, 1453–1440, 1408–1390, 1340, 1284, 1265, 1221, 1196, 1190, 1182, 1145, 1065, 933, 871, 824, 753, 614 cm^{-1}. HRMS (+ESI): Calc. for MH^+, 485.1825. Found, 485.1780.

*[4-(Bis-pyridin-2-ylmethylamino)phenyl](4,5-dimethoxy-2-nitrophenyl)methanol (ZinCast-1, **1**).* Compound **5** (0.875 g, 1.99 mmol) was dissolved in CH_3CN, chilled to 0 °C and $NaBH_4$ (753 mg, 1.99 mmol) was added slowly over a period of 1–2 min. After the addition was complete, the reaction mixture was slowly heated to 70 °C over a period of 2 h and stirred for an additional 12 h. The reaction mixture was diluted into 10 mL of ice water and 1 mL of conc. HCl, and the pH was adjusted to 9 with 6 M NaOH. The product was extracted into CH_2Cl_2 (3 × 30 mL) and the combined organic extracts were dried over Mg_2SO_4. Flash chromatography on alumina (4 : 6 CH_2Cl_2–EtOAc) followed by recrystallization from toluene–hexanes yielded ZinCast-1 as fine yellow crystals (0.324 g, 33.5%).

*(4-Iodophenyl)bis-pyridin-2-ylmethylamine (**17**).* Compound **10** (0.507 g, 1.84 mmol) was dissolved in CH_3CN (10 mL) and chilled to 0 °C. [K(18-crown-6)]ICl_2 (0.970 g, 1.94 mmol) was added and the reaction mixture was stirred at room temperature for 30 min. After removing the solvent, the reaction residue was diluted with 25 mL of water and the pH was adjusted to 9 with 6 M NaOH. The product was extracted into EtOAc (3 × 25 mL), washed with saturated $NaHSO_3$ (25 mL) and brine (3 × 25 mL) the combined organic extracts were dried over $MgSO_4$. Flash chromatography on alumina (1 : 1 hexanes–EtOAc) followed by recrystallization from hexanes yielded **5** as pale yellow needles (0.687 g, 93.0%). Mp 104–105 °C. ^{1}H NMR ($CDCl_3$, 400 MHz) δ 8.59 (2 H, d, J = 8.0 Hz), 7.62 (2 H, t, J = 8.0 Hz), 7.39 (2 H, d, J = 8.0 Hz), 7.22 (2 H, d, J = 4.0 Hz), 7.18 (2 H, t, J = 8.0 Hz), 6.49 (2 H, d, J = 8.0 Hz), 4.79 (4 H, s). ^{13}C NMR ($CDCl_3$, 100 MHz) δ 158.5, 150.1, 148.0, 138.1, 137.1, 122.4, 121.0, 115.1, 78.6, 57.6 ppm. IR (KBr) 3048, 3006, 2927, 1862, 1585, 1494, 1469, 1435, 1383, 1357, 1278, 1254, 1235, 1195, 1177, 1151, 1145, 1090, 1049, 1043, 665, 545, 458 cm^{-1}. HRMS (+ESI): Calc. for MH^+, 402.0467. Found, 402.0458.

*Bis-pyridin-2-ylmethyl[4-(4,4,5,5-tetramethyl-1,3,2-dioxaborolan-2-yl)phenyl]amine (**18**).* Compound **5** (0.307 g, 0.766 mmol), KOAc (0.226 g, 2.30 mmol), $PdCl_2$ (4.1 mg, 3 mol%), PPh_3 (12.1 mg, 6 mol%), bis(pinacolato)diboron ($B(Pin)_2$, 0.214 g, 0.843 mmol) and DMSO (10 mL) were combined in a Schlenk tube. After performing three freeze–pump–thaw cycles, the tube was filled with N_2, sealed and heated at 80 ± 5 °C for 12 h. The mixture was cooled, diluted with H_2O (25 mL) and extracted with EtOAc (3 × 25 mL) and dried with Na_2SO_4. Flash chromatography on alumina (1 : 1 petroleum ether–EtOAc) yielded **6** as a white solid (0.162 g, 52.8%). Mp 201–202 °C. ^{1}H NMR ($CDCl_3$, 400 MHz) δ 8.59 (2 H, d, J = 4.0 Hz), 7.63–7.58 (4 H, m), 7.20 (2 H, d, J = 8.0 Hz), 7.17 (2 H, t, J = 8.0 Hz), 6.69 (2 H, d, J = 8 Hz), 4.85 (4 H, s), 1.29 (12 H, s). ^{13}C NMR ($CDCl_3$, 100 MHz) δ 158.6, 150.7, 150.0, 137.1, 136.6, 122.3, 120.9, 111.9, 83.5, 77.6, 57.2 ppm. IR (KBr) 616, 652, 750, 810, 964, 991, 1141, 1372, 1470, 1606, 2928, 2973, 3046, 3082 cm^{-1}. HRMS (+ESI): Calc. for MH^+, 402.2353. Found, 402.2337.

*[4-(Bis-pyridin-2-ylmethylamino)phenyl](4,5-dimethoxy-2-nitrophenyl)methanol (**1**, ZinCast-1).* Compound **6** (0.150 g, 0.374 mmol), **11** (79.0 mg, 0.374 mmol), tris-1-naphthylphosphine ($P(Nap)_3$), 15.4 mg, 10 mol%), $PdCl_2$ (6.6 mg, 10 mol%), K_2CO_3 (0.155 g, 1.12 mmol) and THF (10 mL) were combined in a Schlenk tube. The tube was sealed and mixture was stirred at 60 ± 5 °C for 60 h. Solvent was removed under reduced pressure and to the resulting dark brown residue was added 50 mL of water, the mixture was extracted with CH_2Cl_2 and dried with $MgSO_4$. Flash chromatography on alumina with EtOAc provided ZinCast-1 as fine yellow crystals (95.2 mg, 52.3%).

*2-Methoxy-*N,N*-bis(pyridine-2-ylmethyl)aniline (**23**).* Synthesis of **23** followed the same procedure as **9** using anisidine (**22**, 2.23 g, 18.2 mmol), pyridinecarboxyl aldehyde (6.14 mL, 54.6 mmol), $NaBH(OAc)_3$ (11.5 g, 54.6 mmol). The product was purified on basic alumina (3 : 7 EtOAc–hexanes) affording a white solid (4.65 g, 83.8%). Mp 76–77 °C. ^{1}H NMR ($CDCl_3$, 400 MHz) δ 8.46 (2 H, d, J = 4 Hz), 7.53 (2 H, t, J = 8 Hz), 7.47 (2 H, d, J = 8 Hz), 7.05 (2 H, t, J = 4 Hz), 6.86 (3 H, m), 6.72 (1 H, m), 4.50 (4 H, s), 3.82 (3 H, s). ^{13}C NMR ($CDCl_3$, 100 MHz) δ 159.9, 152.8, 149.0, 139.3, 136.4, 122.5, 122.4, 121.8, 120.9, 120.8, 111.8, 58.8, 55.6 ppm. IR (KBr) 2840, 1590, 1569, 1502, 1471, 1462, 1436, 1432, 1427, 1352, 1240, 1179, 1154, 1029 cm^{-1}. HRMS (+ESI): Calc. for MH^+, 306.1606. Found, 306.1618.

*4-Bromo-2-methoxy-*N,N*-bis(pyridine-2-ylmethyl)aniline (**24**).* Compound **23** (0.52 g, 1.7 mmol) was dissolved in CH_3CN (10 mL) and [K(18-crown-6)]Br_3 (1.02 g, 1.9 mmol) was added and the reaction mixture was stirred at room temperature for 2 h. After removing the solvent, the reaction residue was diluted with 25 mL of water and the pH was adjusted to 9 with 6 M NaOH. The product was extracted into EtOAc (3 × 25 mL), washed with saturated $NaHSO_3$ (25 mL) and brine (25 mL) the combined organic extracts were dried over $MgSO_4$. Flash chromatography on alumina (3 : 7 EtOAc–hexanes) yielded **24** as white solid (0.638 g, 97.1%). Mp 130–131 °C. ^{1}H NMR ($CDCl_3$, 400 MHz) δ 7.47 (2 H, d, J = 4 Hz), 7.54 (2 H, d, J = 8 Hz), 7.41 (2 H, d,

J = 8 Hz), 7.07 (2 H, t, J = 8 Hz), 6.94 (1 H, s), 6.82 (1 H, d, J = 8 Hz), 6.70 (1 H, d, J = 8 Hz), 4.46 (4 H, s), 3.81 (3 H, s). ^{13}C NMR ($CDCl_3$, 100 MHz) δ 159.3, 153.5, 149.1, 138.5, 136.5, 123.6, 122.3, 122.1, 122.0, 115.2, 114.6, 58.7, 55.9 ppm. IR (KBr) 2840, 1589, 1568, 1496, 1476, 1457, 1444, 1398, 1375, 1351, 1322, 1273, 1237, 1191, 1176, 1153, 1121, 1025 cm^{-1}. HRMS (+ESI): Calc. for MH$^+$, 384.0711. Found, 384.0736.

2-Methoxy-N,N-*bis(pyridine-2-ylmethyl)-4-(tetramethyl-1,3,2-dioxaborolan-2-yl)aniline* ***(25)***. Compound **24** (0.51 g, 1.3 mmol), KOAc (0.0.39 g, 3.9 mmol), Pd_2dba_3 (15 mg, 2 mol %), DavePhos (21 mg, 4 mol%), $B(Pin)_2$ (1.01 g, 3.9 mmol) and dioxane (15 mL) were combined in a Schlenk tube. After performing three freeze–pump–thaw cycles, the tube was filled with N_2, sealed and heated at 110 ± 5 °C for 48 h. The mixture was cooled, washed with H_2O (2 × 15 mL) and dried with Na_2SO_4. Flash chromatography on alumina (2 : 3 EtOAc–hexanes) yielded **25** as white solid (0.549 g, 96.5%). Mp 98–99 °C. ^{1}H NMR ($CDCl_3$, 400 MHz) δ 7.47 (2 H, d, J = 8 Hz), 7.53 (2 H, t, 8 Hz), 7.41 (2 H, d, J = 12 Hz), 2.23 (2 H, m), 7.06 (2 H, t, J = 8 Hz), 6.80 (1 H, d, J = 8 Hz), 4.56 (4 H, s), 3.84 (3 H, s), 1.28 (12 H, s). ^{13}C NMR ($CDCl_3$, 100 MHz) δ 159.6, 151.6, 149.0, 142.2, 136.5, 128.3, 122.2, 121.9, 119.4, 117.4, 100.1, 83.7, 58.5, 55.7, 25.0 ppm. IR (KBr) 2975, 1602, 1591, 1568, 1513, 1472, 1432, 1408, 1382, 1372, 1348, 1273, 1231, 1175, 1157, 1142, 1103, 1033, 965, 854, 769, 687 cm^{-1}. HRMS (+ESI): Calc. for MH$^+$, 432.2458. Found, 432.2448.

{4-[Bis(lyridin-2-ylmethyl)amino]-3-methoxyphenyl}(4,5-dimethoxy-2-nitrophenyl)methanol ***(26, ZinCast-4)***. Synthesis of ZinCast-4 followed the same procedure as ZinCast-1. Compound **26** (1.00 g, 2.32 mmol), **11** (0.49 g, 2.32 mmol), $P(Nap)_3$ (96 mg, 10 mol%), $PdCl_2$ (41 mg, 10 mol%), K_2CO_3 (0.96 g, 6.96 mmol). The product was purified on silica (1 : 19 CH_3OH–EtOAc) affording yellow solid (0.509 g, 43.0%). Mp 180–182 °C. ^{1}H NMR ($CDCl_3$, 400 MHz) δ 8.44 (2 H, d, J = 4 Hz), 7.54 (3 H, m), 7.42 (2 H, d, J = 8 Hz), 7.19 (1 H, s), 7.06 (2 H, t, J = 8 Hz), 6.92 (1 H, s), 6.75 (1 H, d, J = 8 Hz), 6.58 (1 H, d, J = 8 Hz), 6.42 (1 H, s), 4.45 (4 H, s), 3.91 (3 H, s), 3.86 (3 H, s), 3.78 (3 H, s), 3.28 (1 H, s). ^{13}C NMR ($CDCl_3$, 100 MHz) δ 159.7, 153.5, 152.5, 149.0, 148.0, 140.5, 139.0, 136.5, 136.1, 134.5, 122.4, 121.9, 120.3, 119.1, 111.1, 110.7, 108.2, 71.4, 58.6, 56.6, 56.5, 55.7 ppm. IR (KBr) 3269, 3009, 2936, 2835, 1591, 1571, 1519, 1466, 1439, 1431, 1325, 1273, 1256, 1218, 1159, 1067, 1034, 797, 765, 745 cm^{-1}. HRMS (+ESI): Calc. for MH$^+$, 517.2087. Found, 517.2070.

5-Iodo-2-methoxy-N,N-*bis(pyridine-2-ylmethyl)aniline* ***(28)***. To a solution of 5-iodo-2-methoxyaniline (**27**, 1.00 g, 4.02 mmol) in CH_3CN (40 mL) was added 2-(bromomethyl)pyridine hydrobromide (4.05 g, 16.1 mmol), potassium hydrogen phosphate (K_2HPO_4) (2.80 g, 16.1 mmol) and KI (0.33 g, 2.01 mmol). After the reaction mixture was refluxed overnight, the solvent was removed, 20 mL of water was added and pH was adjusted to ~9. The crude product was extracted with EtOAc (3 × 20 mL) and dried over $MgSO_4$. Flash chromatography on basic alumina (2 : 3 EtOAc–hexanes) yielded product as yellow oil (1.09 g, 63.0%). ^{1}H NMR ($CDCl_3$, 400 MHz) δ 8.48 (2 H, d, J = 4 Hz), 7.56 (2 H, t, J = 8 Hz), 7.41 (2 H, d, J = 8 Hz), 7.15 (2 H, m), 7.08 (2 H, t, J = 8 Hz), 6.57 (1 H, d, J = 8 Hz), 4.47 (4 H, s), 3.77 (3 H, s). ^{13}C NMR ($CDCl_3$, 100 MHz) δ 159.2, 152.8, 149.2, 141.2, 136.5, 131.2, 129.5, 122.3, 122.0, 113.7, 83.3, 58.5, 55.7 ppm. IR 1589, 1569, 1494, 1462, 1433, 1402, 1375, 1296, 1239, 1178, 1148, 1094, 1047, 1024, 994, 943, 798, 761 cm^{-1}. HRMS (+ESI): Calc. for MH$^+$, 432.0573. Found, 432.0572.

2-Methoxy-N,N-*bis(pyridine-2-ylmethyl)-5-(tetramethyl-1,3,2-dioxoborolan-2-yl)aniline* ***(29)***. Synthesis of **29** followed the same procedure as compound **18** using **28** (0.20 g, 0.46 mmol), KOAc (0.14 g, 1.38 mmol), $PdCl_2$ (2.5 mg, 3 mol%), PPh_3 (7.3 mg, 6 mol%), $B(Pin)_2$ (0.13 g, 0.51 mmol). The product was purified on basic alumina (6 : 13 EtOAc–hexanes) affording yellow solid (0.45 g, 51%). Mp 151–152 °C. ^{1}H NMR ($CDCl_3$, 400 MHz) δ 8.45 (2 H, d, J = 8 Hz), 7.52 (4 H, m), 7.40 (2 H, m), 7.04 (2 H, m), 6.85 (1 H, d, J = 8 Hz), 4.49 (4 H, s), 3.83 (3 H, s), 1.25 (12 H, s). ^{13}C NMR ($CDCl_3$, 100 MHz) δ 160.1, 156.0, 148.9, 139.1, 136.4, 130.4, 127.7, 122.5, 121.7, 111.1, 83.6, 58.9, 55.5, 25.0 ppm. IR (KBr) 3060, 2975, 2931, 2837, 1571, 1510, 1472, 1381, 1354, 1316, 1296, 1270, 1238, 1198, 1175, 1141, 1125, 1101, 1054, 1043, 1023, 996, 963, 949, 887, 851, 813, 773, 759. HRMS (+ESI): Calc. for MH$^+$, 432.2458. Found, 432.2434.

{3-[Bis(pyridine-2-ylmethyl)amino]-4-methoxyphenyl}(4,5-dimethoxy-2-nitrophenyl)methanol ***(30, ZinCast-5)***. Compound **29** (0.35 g, 0.82 mmol), **11** (0.17 g, 0.82 mmol), $P(Nap)_3$ (34 mg, 10 mol%), $PdCl_2$ (15 mg, 10 mol%), K_2CO_3 (0.40 g, 2.46 mmol). The product was purified on basic alumina (1 : 9 hexanes–EtOAc) affording yellow solid (0.12 g, 30%). Mp 135–136 °C. ^{1}H NMR ($CDCl_3$, 400 MHz) δ 8.39 (2 H, d, J = 8 Hz), 7.50 (3 H, t, J = 8 Hz), 7.37 (2 H, d, J = 8 Hz), 7.12 (1 H, s), 7.03 (2 H, t, J = 2 Hz), 6.91 (1 H, d, J = 8 Hz), 6.79 (1 H, d, J = 8 Hz), 6.70 (1 H, s), 6.30 (1 H, d, J = 4 Hz), 5.28 (2 H, s), 4.42 (4 H, t, J = 16 Hz), 3.92 (3 H, s), 3.86 (3 H, s), 3.79 (3 H, s), 2.80 (1 H, s). ^{13}C NMR ($CDCl_3$, 100 MHz) δ 159.6, 153.4, 152.3, 148.9, 147.8, 140.0, 139.3, 136.4, 134.6, 134.4, 122.3, 121.8, 121.2, 119.5, 111.4, 110.3, 108.1, 71.41, 58.68, 56.54, 55.71 ppm. Ir (KBr) 3107, 2939, 1596, 1569, 1521, 1507, 1471, 1433, 1360, 1335, 1276, 1248, 1235, 1211, 1186, 1159, 1145, 1115, 1095, 1066, 1047, 1028, 1005, 986, 972, 949, 889, 817, 797, 772, 753, 747, 734 cm^{-1}. HRMS (+ESI): Calc. for MH$^+$, 517.2087. Found, 517.2103.

(4,5-Dimethoxy-2-nitrophenyl)(2-methoxyphenyl)methanol (m-*OMeCast,* ***33)***. 3-Methoxyphenylboronic acid (**31**, 0.73 g, 0.4.68 mmol), **11** (0.54 g, 2.34 mmol), $P(Nap)_3$ (48 mg, 5 mol %), $PdCl_2$ (21 mg, 5 mol%), K_2CO_3 (0.155 g, 1.12 mmol) and THF (10 mL) were combined in a Schlenk tube. The tube was sealed and mixture was stirred at 65 ± 5 °C for 24 h. The reaction mixture was cooled, filtered and solvent was removed. Flash chromatography on silica (2 : 3 EtOAc–hexanes) yielded a yellow solid (0.435 g, 58.2%). Mp 83–84 °C. ^{1}H NMR ($CDCl_3$, 400 MHz) δ 7.61 (1 H, s), 7.25 (2 H, m), 6.90 (2 H, m), 6.82 (1 H, d, J = 8 Hz), 6.50 (1 H, s), 3.94 (6 H, d, J = 8 Hz), 3.79 (3 H, s), 2.88 (1 H, s). ^{13}C NMR ($CDCl_3$, 100 MHz) δ 159.9, 153.6, 148.2, 143.6, 140.6, 134.0, 129.7, 119.4, 113.4, 112.9, 110.9, 108.3, 71.7, 56.6, 55.4 ppm. IR (KBr) 3543, 1605, 1580, 1513, 1503, 1488, 1463, 1447, 1436, 1399, 1329, 1264, 1207, 1182, 1161, 1146, 1059, 1048, 1017, 987, 891, 880, 869, 788, 780 cm^{-1}. HRMS (+ESI): Calc. for MH$^+$, 302.1028. Found, 302.1028.

(4,5-Dimethoxy-2-nitrophenyl)([2-(dimethylamino)phenyl]methanol (m-*DMACast,* ***34)***. The synthesis of **16** followed the same

procedure as compound **34**. 3-(*N*,*N*-Dimethylamino)boronic acid (**32**, 0.32 g, 1.94 mmol), **11** (0.21 g, 0.97 mmol), $P(Nap)_3$ (20 mg, 5 mol%), $PdCl_2$ (8.6 mg, 5 mol%), K_2CO_3 (0.40 g, 2.91 mmol). The product was purified on basic alumina (1 : 1EtOAc–hexanes) affording orange oil (0.754 g, 79.6%). ^{1}H NMR ($CDCl_3$, 400 MHz) δ 7.58 (1 H, s), 7.15 (1 H, t, J = 8 Hz), 6.76 (1 H, s), 6.63 (1 H, d, J = 8 Hz), 6.58 (1 H, d, J = 8 Hz), 6.45 (1 H, d, J = 4 Hz), 3.91 (6 H, d, J = 4 Hz), 2.91 (6 H, s), 2.77 (1 H, d, J = 4 Hz). ^{13}C NMR ($CDCl_3$, 100 MHz) δ 153.5, 150.9, 148.1, 142.9, 140.6, 134.3, 129.4, 114.9, 112.3, 111.5, 110.9, 108.2, 72.1, 56.5, 40.7 ppm. IR (KBr) 3514, 2935, 1601, 1578, 1514, 1460, 1436, 1328, 1266, 1212, 1151, 1059, 1030, 993, 964, 866, 795, 764, 732, 696. HRMS (+ESI): Calc. for MH^+, 333.1450. Found, 333.1436.

General procedure for synthesis of ZinUnc compounds. A solution of ZinCast in CH_3CN (0.03 M) was placed in a quartz cuvette and irradiated for ~12 h with a 1000 W Xe lamp. The resulting solution was evaporated to dryness and purified by flash chromatography on basic alumina (3 : 10 hexanes–EtOAc).

4-[(4,5-Dimethoxy-2-nitrosophenyl)carbonyl]-N-*[2-(pyridine-2-yl)ethyl]*-N-*(pyridine-2-ylmethyl)aniline (**12**, ZinUnc-2).* Photolysis of **3** (50 mg, 0.10 mmol) followed by chromatography lead to isolation of ZinUnc-2 as a green solid (23 mg, 48%). Mp 137–139 °C. ^{1}H NMR ($CDCl_3$, 400 MHz) δ 8.52 (2 H, d, J = 4 Hz), 7.70 (2 H, d, J = 8 Hz), 7.55 (2 H, q, J = 8 Hz), 7.10 (4 H, m), 7.01 (1 H, d, J = 8 Hz), 6.65 (2 H, d, J = 8 Hz), 6.29 (1 H, s), 4.59 (2 H, s), 3.98 (5 H, m), 3.88 (3 H, s), 3.13 (2 H, t, J = 8 Hz). ^{13}C NMR ($CDCl_3$, 100 MHz) δ 194.0, 160.1, 158.8, 157.8, 156.0, 152.2, 150.2, 150.0, 149.9, 140.3, 137.1, 136.8, 132.9, 127.6, 123.8, 122.4, 121.9, 120.6, 111.3, 109.8, 91.8, 57.0, 56.9, 56.4, 51.9, 35.9 ppm. IR (KBr) 1651, 1602, 1591, 1566, 1556, 1523, 1509, 1469, 1444, 1432, 1386, 1358, 1326, 1299, 1260, 1224, 1196, 1146, 1083 cm^{-1}. HRMS (+ESI): Calc. for MH^+, 483.2027. Found, 483.2006.

4-[(4,5-Dimethoxy-2-nitrosophenyl)carbonyl]-N,N-*bis[2-(pyridine-2-yl)ethyl]aniline (**13**, ZinUnc-3).* Photolysis of **4** (50 mg, 0.097 mmol) followed by chromatography lead to isolation of ZinUnc-3 as a green solid (22 mg, 46%). Decomp. 99–101 °C. ^{1}H NMR ($CDCl_3$, 400 MHz) δ 8.52 (2 H, d, J = 4 Hz), 7.74 (2 H, d, J = 8 Hz), 7.54 (2 H, t, J = 8 Hz), 7.07 (5 H, m), 6.70 (2 H, d, J = 8 Hz), 6.30 (1 H, s), 4.02 (3 H, s), 3.89 (3 H, s), 3.70 (4 H, t, J = 8 Hz); 3.98 (4 H, t, J = 8 Hz). ^{13}C NMR ($CDCl_3$, 100 MHz) δ 193.9, 160.1, 158.9, 156.0, 151.8, 150.1, 149.8, 140.5, 136.7, 133.0, 126.9, 123.7, 121.8, 110.9, 109.9, 91.7, 57.0, 56.4, 51.2, 35.9 ppm. IR (KBr) 2362, 1645, 1595, 1509, 1471, 1443, 1257, 1224, 1148, 1079 cm^{-1}. HRMS (+ESI): Calc. for MH^+, 497, 2183. Found, 497.2170.

4-[(4,5-Dimethoxy-2-nitrophenyl)carbonyl]-N,N-*dimethylaniline (**21**, DMAUnc).* Photolysis of DMACast (**20**, 6.4 mg, 0.020 mmol) followed by chromatography yielded yellow solid (3.0 mg, 49%). Mp 166–168 °C. ^{1}H NMR ($CDCl_3$, 400 MHz) δ 7.73 (2 H, d, J = 8 Hz), 7.12 (1 H, s), 6.58 (2 H, d, J = 8 Hz), 6.30 (1 H, s), 4.01 (3 H, s), 3.89 (3 H, s), 3.03 (6 H, s). ^{13}C NMR ($CDCl_3$, 100 MHz) δ 194.0, 160.0, 155.9, 154.0, 150.1, 140.3, 132.6, 126.8, 110.7, 109.9, 91.7, 56.9, 56.4, 40.2 ppm. IR (KBr) 1587, 1508, 1452, 1433, 1319, 1296, 1255, 1226, 1192, 1183, 1142, 1079, 895, 817, 750 cm^{-1}. HRMS (+ESI): Calc. for MH^+, 315.1345. Found, 315.1369.

4-[(4,5-Dimethoxy-2-nitrosophenyl)carbonyl]-2-methoxy-N,N-*bis(pyridine-2-ylmethyl)aniline (**35**, ZinUnc-4).* Photolysis of ZinCast-4 (53 mg, 0.10 mmol) followed by chromatography yielded yellow solid (21 mg, 41%). Decomp. 78–80 °C. ^{1}H NMR ($CDCl_3$, 400 MHz) δ 8.48 (2 H, d, J = 4 Hz), 7.66 (1 H, s), 7.59 (2 H, J = 8 Hz), 7.36 (2 H, d, J = 8 Hz), 7.09 (3 H, m), 6.95 (1 H, d, J = 8 Hz), 6.66 (1 H, d, J = 8 Hz), 6.33 (1 H, s), 4.68 (4 H, s), 4.00 (3 H, s), 3.88 (3 H, s), 3.78 (3 H, s). ^{13}C NMR ($CDCl_3$, 100 MHz) δ 194.6, 160.0, 158.9, 155.9, 151.0, 150.3, 149.4, 145.2, 139.3, 136.8, 131.3, 126.8, 122.2, 121.8, 117.2, 111.3, 109.8, 92.3, 58.3, 57.0, 56.4, 55.9 ppm. IR (KBr) 2361, 1645, 1594, 1508, 1471, 1442, 1256, 1223, 1148, 1079, 857, 750. HRMS (+ESI): Calc. for MH^+, 499.1981. Found, 499.2020.

Spectroscopy. Absorption spectra were recorded on a Cary 50 UV-visible spectrophotometer run under Varian's Cary WinUV software. Analytical photolysis reactions were performed on a Hitachi F-4500 spectrophotometer run under FL Solutions 2.0 software and equipped with 150 W Xe lamp and 700 V photomultiplier tube. All spectra were acquired at 25 °C in quartz cuvettes with path length of 1 cm and cell volume of 3.0 mL. Stock solutions of ZinCast photocages was prepared at mM concentrations in DMSO and diluted to prepare 25 μM solutions in the solvent of choice. All metal binding constants and quantum yields for first-generation ZinCast photocages were determined by previously described procedures.[11,17,33,34]

Binding constants. Stock solutions of ZinCast-1, -2, -3, -4 or -5, ZinUnc-1, -2, -4 or -3 and the metal perchlorate salts of Cu^{2+}, Zn^{2+} and Cd^{2+} were prepared in mM concentration in spectrophotometric grade CH_3CN. A 25 μM solution of the ligand was prepared in 3000 μL of the solvent and titrated in triplicate with each of the metal salt stock solutions. Absorbance spectra were corrected for dilution and the conditional dissociation constant (K_d) was calculated using XLfit.[14]

Quantum yields. Photochemistry of the second generation photocages was evaluated by irradiating 0.25 mM solutions prepared in HPLC grade CH_3CN with a 150 W source at 350 nm. The change in concentration of ZinCast-1, -2, -3 DMACast was evaluated by UV-vis spectroscopy by monitoring the absorption increase at ~350 nm. For ZinCast-4, -5, *m*-OMeCast and *m*-DMACast the photolysis was followed with an Agilent 1100 HPLC equipped with a Grace Apollo 5 μm silica 4.6 × 250 mm column as previously described.[29] *m*-OMeCast and *m*-DMACast were eluted with 5 to 7% iPrOH–hexanes gradient elution, while ZinCast-4 and ZinCast-5 were eluted with 5% iPrOH–EtOAc and 15% iPrOH–EtOAc, respectively. Quantum yields were calculated with the following formula:

$$\Phi = \frac{(\Delta[\text{cage}]/\Delta t)}{I} N_A$$

where I is source intensity measured by iron oxalate actinometry and N_A is Avogadro's number.

Collection and reduction of X-ray data

Structural analysis was carried out in the X-Ray Crystallographic Facility at Worcester Polytechnic Institute. A colorless plate of [Zn(**23**)]Cl_2 having approximate dimensions of 0.02 × 0.10 × 0.20 mm was covered in paratone oil on 100 μ MiTeGen polyimide micromounts was mounted on a Bruker-AXS APEX CCD

Table 6 Crystallographic parameters for [Zn(**23**)]Cl_2

Formula	$ZnCl_2N_3OC_{19}H_{19}$
M_r	441.64
Space group	$P2_1/c$
a/Å	7.7523(3)
b/Å	25.2982(11)
c/Å	10.7609(4)
β/°	106.849(2)
V/Å^3	2019.82
Z	4
D_c/g cm^{-3}	1.452
μ/cm^{-1}	1.493
T/K	100(2)
Total no. data	17 291
No. unique data	3997
Obs. data[a]	2910
No. parameters	236
R^b	0.0608
w$R_2{}^c$	0.0756
Max., min. peaks/e Å^{-3}	0.569, −0.264

[a] Observation criterion: $I > 2\sigma(I)$. [b] $R = \sum||F_o| - |F_c||/\sum|F_o|$. [c] $wR_2 = [\sum(w(F_o^2 - F_c^2)^2)/\sum w(F_o^2)^2]^{1/2}$.

Table 7 Selected bond lengths (Å) and angles (°) for [Zn(**23**)]Cl_2 with estimated standard deviations in parentheses

Zn(1)–N(1)	2.098(2)	Zn(1)–N(2)	2.105(2)
Zn(1)–N(4)	2.414(2)	Zn(1)–Cl(1)	2.2944(7)
Zn(1)–Cl(2)	2.2711(9)		
N(1)–Zn(1)–N(2)	141.15(8)	N(1)–Zn(1)–N(4)	73.52(8)
N(1)–Zn(1)–Cl(1)	102.04(6)	N(1)–Zn(1)–Cl(2)	99.86(6)
N(2)–Zn(1)–N(4)	73.65(8)	N(2)–Zn(1)–Cl(1)	101.99(6)
N(2)–Zn(1)–Cl(2)	98.36(6)	N(4)–Zn(1)–Cl(1)	96.93(5)
N(4)–Zn(1)–Cl(2)	150.25(6)	Cl(1)–Zn(1)–Cl(2)	112.81(3)

diffractometer equipped with an LT-II low-temperature device. Diffraction data were collected at 100(2) K using graphite monochromated Mo-Kα radiation (λ = 0.71073 Å) using the omega scan technique. Empirical absorption corrections were applied using the SADABS program.[35] The unit cells and space groups were determined using the SAINT+ program.[35] The structures were solved by direct methods and refined by full matrix least-squares using the SHELXTL program.[35] Refinement was based on F^2 using all reflections. All non-hydrogen atoms were refined anisotropically. Hydrogen atoms on carbon atoms were all located in the difference maps and subsequently placed at idealized positions and given isotropic U values 1.2 times that of the carbon atom to which they were bonded. Hydrogen atoms bonded to oxygen atoms were located and refined with isotropic thermal parameters. Mercury 1.4.2 software was used to examine the molecular structure.[36] The crystallographic data and refinement parameters for [Zn(**23**)]Cl_2 are given in Table 6 with selected bond lengths and angles in Table 7. The 50% thermal ellipsoid plot is shown in Fig. 5.

Acknowledgements

This work was supported by the Worcester Polytechnic Institute and by NSF grant CHE-0955361 and C. V. S. by NSF-REU program (CHE-0754580).

Notes and references

1 G. Mayer and A. Heckel, *Angew. Chem., Int. Ed.*, 2006, **45**, 4900–4921.
2 K. L. Ciesienski and K. J. Franz, *Angew. Chem., Int. Ed.*, 2011, **50**, 814–824.
3 G. C. Ellis-Davies, *Nat. Methods*, 2007, **4**, 619–628.
4 S. Adams and R. Tsien, *Annu. Rev. Physiol.*, 1993, **55**, 755–784.
5 E. Neher, *Neuron*, 1998, **20**, 389–399.
6 G. C. R. Ellis-Davies, *Chem. Rev.*, 2008, **108**, 1603–1613.
7 E. L. Que, D. W. Domaille and C. J. Chang, *Chem. Rev.*, 2008, **108**, 1517–1549.
8 P. Paoletti, A. M. Vergnano, B. Barbour and M. Casado, *Neuroscience*, 2009, **158**, 126–136.
9 M. D. Pluth, E. Tomat and S. J. Lippard, *Annu. Rev. Biochem.*, 2011, **80**, 333–355.
10 H. M. Bandara, D. P. Kennedy, E. Akin, C. D. Incarvito and S. C. Burdette, *Inorg. Chem.*, 2009, **48**, 8445–8455.
11 C. Gwizdala, D. P. Kennedy and S. C. Burdette, *Chem. Commun.*, 2009, 6967–6969.
12 H. M. D. Bandara, T. P. Walsh and S. C. Burdette, *Chem.–Eur. J.*, 2011, **17**, 3932–3941.
13 R. Y. Tsien and R. S. Zucker, *Biophys. J.*, 1986, **50**, 843–853.
14 *XLfit*, 5.1.0.0, ID Business Solutions Limited, Guildford, UK, 2009.
15 J. Corrie, A. Barth, V. Munasinghe, D. Trentham and M. Hutter, *J. Am. Chem. Soc.*, 2003, **125**, 8546–8554.
16 M. Gaplovsky, Y. V. Il'ichev, Y. Kamdzhilov, S. V. Kombarova, M. Mac, M. A. Schworer and J. Wirz, *Photochem. Photobiol. Sci.*, 2005, **4**, 33–42.
17 D. P. Kennedy, C. Gwizdala and S. C. Burdette, *Org. Lett.*, 2009, **11**, 2587–2590.
18 F. P. Hinz and D. W. Margerum, *J. Am. Chem. Soc.*, 1974, **96**, 4993–4994.
19 Y. Gultneh, A. R. Khan, D. Blaise, S. Chaudhry, B. Ahvazi, B. B. Marvey and R. J. Butcher, *J. Inorg. Biochem.*, 1999, **75**, 7–18.
20 K. Choi, H. Ryu, N. Sung and M. Suh, *J. Chem. Crystallogr.*, 2003, **33**, 947–950.
21 H. C. Brown, D. H. McDaniel and O. Hafliger, in *Determination of Organic Structures by Physical Methods*, ed. P. Haflinger, E. A. Braude and F. C. Nachod, Academic Press, New York, NY, 1955.
22 M. M. Fickling, A. Fischer, B. R. Mann, J. Packer and J. Vaughan, *J. Am. Chem. Soc.*, 1959, **81**, 4226–4230.
23 R. Hancock, P. Wade, M. Ngwenya, A. Desousa and K. Damu, *Inorg. Chem.*, 1990, **29**, 1968–1974.
24 A. Hazell, C. McKenzie and L. Nielsen, *J. Chem. Soc., Dalton Trans.*, 1998, 1751–1756.
25 S. Foxon, J. Xu, S. Turba, M. Leibold, F. Hampel, F. W. Heinemann, O. Walter, C. Wuertele, M. Holthausen and S. Schindler, *Eur. J. Inorg. Chem.*, 2007, 429–443.
26 Y. Zhang, L. Chen, W. Yin, J. Yin, S. Zhang and C. Liu, *Dalton Trans.*, 2011, **40**, 4830–4833.
27 M. Taki, Y. Watanabe and Y. Yamamoto, *Tetrahedron Lett.*, 2009, **50**, 1345–1347.
28 S. Iyoshi, M. Taki and Y. Yamamoto, *Org. Lett.*, 2011, **13**, 4558–4561.
29 D. P. Kennedy, D. C. Brown and S. C. Burdette, *Org. Lett.*, 2010, **12**, 4486–4489.
30 Y. Lee, G. Y. Park, H. R. Lucas, P. L. Vajda, K. Kamaraj, M. A. Vance, A. E. Milligan, J. S. Woertink, M. A. Siegler, A. A. N. Sarjeant, L. N. Zakharov, A. L. Rheingold, E. I. Solomon and K. D. Karlin, *Inorg. Chem.*, 2009, **48**, 11297–11309.
31 T. Sakamoto, H. Nagata, Y. Kondo, K. Sato and H. Yamanaka, *Chem. Pharm. Bull.*, 1984, **32**, 4866–4872.
32 I. Sanyal, M. Mahroof-Tahir, M. S. Nasir, P. Ghosh, B. I. Cohen, Y. Gultneh, R. W. Cruse, A. Farooq and K. D. Karlin, *Inorg. Chem.*, 1992, **31**, 4322–32.
33 H. W. Mbatia, D. P. Kennedy, C. E. Camire, C. D. Incarvito and S. C. Burdette, *Eur. J. Inorg. Chem.*, 2010, **2010**, 5069–5078.
34 D. P. Kennedy, C. D. Incarvito and S. C. Burdette, *Inorg. Chem.*, 2010, **49**, 916–923.
35 *Bruker SAINT 6.14 and SHELXTL 6.14 for WNT/2003*, Bruker AXS Inc., Madison, WI, 1999.
36 *CCDC Mercury 1.4.2*, CCDC, Cambridge, UK, 2009.

